

The Structures of Distant Galaxies - III: The Merger History of over 20,000 Massive Galaxies at $z < 1.2$

Christopher J. Conselice^{1*}, Cui Yang¹, Asa F. L. Bluck¹

¹ *University of Nottingham, School of Physics & Astronomy, Nottingham, NG7 2RD UK*

Accepted ; Received ; in original form

ABSTRACT

Utilizing deep Hubble Space Telescope imaging from the two largest field galaxy surveys, the Extended Groth Strip (EGS) and the COSMOS survey, we examine the structural properties, and derive the merger history for 21,902 galaxies with $M_* > 10^{10} M_\odot$ at $z < 1.2$. We examine the structural CAS parameters of these galaxies, deriving merger fractions, at $0.2 < z < 1.2$, based on the asymmetry and clumpiness values of these systems. We find that the merger fraction between $z = 0.2$ and $z = 1.2$ increases from roughly $f_m = 0.04 \pm 0.01$ to $f_m = 0.13 \pm 0.01$. We furthermore detect, at a high significance, an abrupt drop in the merger fraction at $z < 0.7$, which appears relatively constant from $z = 0.7$ to $z = 1.2$. We explore several fitting formalisms for parameterising the merger fraction, and compare our results to other structural studies and pair methods within the DEEP2, VVDS, and COSMOS fields. We also examine the basic features of these galaxies, including our selection for mergers, and the inherent error budget and systematics associated with finding mergers through structure. We find that for galaxies selected by $M_* > 10^{10} M_\odot$, the merger fraction can be parameterised by $f_m = f_0 \times (1+z)^m$ with the power-law slope $m = 2.3 \pm 0.4$. By using the best available $z = 0$ prior the slope increases to $m = 3.8 \pm 0.2$, showing how critical the measurement of local merger properties are for deriving the evolution of the merger fraction. We furthermore show that the merger fraction derived through structure is roughly a factor of 3-6 higher than pair fractions. Based on the latest cosmological simulations of mergers we show that this ratio is predicted, and that both methods are likely tracing the merger fraction and rate properly. We calculate, utilising merger time scales from simulations, and previously published merger fractions within the Hubble Deep and Ultra Deep Fields, that the merger rate of galaxies with $M_* > 10^{10} M_\odot$ increases linearly between $z = 0.7$ and $z = 3$. Finally, we show that a typical galaxy with a stellar mass of $M_* > 10^{10} M_\odot$ undergoes between 1-2 major mergers at $z < 1.2$.

Key words: Galaxies: Evolution, Formation, Structure, Morphology, Classification

1 INTRODUCTION

Unlike the case for stars, the relative size and separation between galaxies is small, suggesting that galaxy interactions and mergers could be a major process in driving galaxy formation. Observational attempts to determine the role of galaxy mergers in the local universe have been limited to studies of how star formation and black hole growth are induced by the merger process (e.g., Barton et al. 2000; Ellison et al. 2008). It is however clear that ongoing major galaxy merging is rare in the nearby universe, and is likely not a dominant mode for the future evolution of galaxies

(e.g., Patton et al. 2000). If galaxy mergers play a major role in galaxy formation they must have occurred earlier in the history of the universe.

Attempts to trace the merger history in the early universe has been carried out using two primary methods. The oldest method involves measuring the fraction of galaxies which are in physical pairs at various look-back times, or redshifts (e.g., Patton et al. 2002; Le Fevre et al. 2000; Lin et al. 2004; Lin et al. 2008; Bluck et al. 2008). A newer method, with a considerable background history (e.g., Holmberg 1941; Vorontsov-Velyaminov 1959; Arp 1966), uses the structures of galaxies to determine the merger history (e.g., Conselice 2003; Conselice et al. 2003; Lotz et al. 2008). It is, however, not yet known if the two methods are revealing

* E-mail: conselice@nottingham.ac.uk

the same merger history for galaxies, although at $z \sim 0$, the agreement between the two methods appears good (e.g., De Propriis et al. 2007).

The merger history of galaxies is still largely only beginning to be measured with some certainty. Two issues that still need to be addressed are the reliability of the current methods for determining merger histories, and the relatively small areas thus far used to find mergers. Both of these issues limit our ability to accurately measure the merger history. The reliability argument has been addressed in great detail in papers such as Conselice (2003), Conselice et al. (2003), Conselice et al. (2005), and Lotz et al. (2004). Briefly, the merger history can only be measured using special techniques and data, such as complete redshift surveys and/or deep Hubble Space Telescope (HST) imaging. It turns out that when examining galaxies that fit a structural merger criteria, nearly all are ongoing major mergers, as judged by eye and through kinematics (e.g., Conselice 2000a,b; Conselice 2003; Conselice et al. 2008). This holds for low and high redshift galaxies (e.g., Conselice et al. 2003), and is also seen when examining N-body models of the merging process (Conselice 2006; Lotz et al. 2008b).

Using structure to determine the merger history requires the use of HST imaging or adaptive optics (AO). However, the small fields of view used in HST and AO surveys make it difficult to measure the merger history with a high certainty, simply due to the small number of galaxies that have been examined. Another issue is that it is difficult to measure the merger history at higher redshifts due to the fact that there is very little high resolution deep near-infrared imaging, which is needed to directly study the rest-frame optical structures of $z > 1.2$ galaxies. This is required, as the rest-frame optical appearance of a galaxy often differs significantly from the rest-frame ultraviolet morphology (e.g., Windhorst et al. 2002; Taylor-Mager et al. 2007). Ideally in the future, using multiple band data, it is desirable to measure parameters and structures on stellar mass images (e.g., Lanyon-Foster et al. 2009).

For our merger measurements, we utilise the CAS method (e.g., Conselice 2003) for determining the presence of galaxy mergers in the galaxy population at $z < 1$. We first re-evaluate the use of the asymmetry index (Conselice et al. 2000a), and the CAS method itself for locating major mergers. We furthermore use our derived merger fractions to characterise the major galaxy merger evolution for $M_* > 10^{10} M_\odot$ galaxies at $z < 3$. We discuss various ways in which this merger evolution can be parameterised, investigating power-law, exponential, and the combination of the two forms. We conclude that the use of a $z = 0$ prior in fitting the merger fraction is a significant factor in the determination of the power-law slope m . We show that this value of m can vary between $m = 1.5$ and $m = 4$ depending on how the merger fraction is fit (cf. Bluck et al. 2008 for ultra massive galaxies).

In this paper we use the two largest HST Advanced Camera for Surveys (ACS) imaging data sets - the Extended Groth Strip (EGS) and the Cosmic Evolution Survey (COSMOS) to determine, using $> 20,000$ massive galaxies, the detailed merger history at $z < 1.2$. This is an important epoch for measuring the merger history, and there is still considerable uncertainty regarding the merging history during this epoch, which traces the last half of the universe.

By using ACS F814W band images we are also tracing the structures of these galaxies in the rest-frame optical out to $z \sim 1$ and do not need to consider the sometimes considerable morphological k -corrections when imaging galaxies in the ultraviolet (e.g., Taylor-Mager et al. 2007).

Our general conclusion is that the merger fraction increases with higher redshifts to $z \sim 1.2$. We use the latest model based time-scales for galaxies in pairs to merge, and for galaxies to remain symmetric during mergers, to calculate the number of mergers a typical $M_* > 10^{10} M_\odot$ galaxy will undergo at $z < 3$, as well as the galaxy merger rate. We conclude that a typical $M_* > 10^{10} M_\odot$ galaxy will undergo 1-2 major mergers at $z < 1$. We also investigate how structural merger fractions compare with pair fractions, finding that at a given redshift, within the same population of galaxies, the CAS merger fraction is 3-6 times higher than the pair fraction. We show that the ratio of the time-scales for CAS mergers and 20 kpc pairs is nearly the same as the merger-pair fraction ratio. Both methods therefore appear to trace the same merging population at different phases. This is further evidence that we are indeed measuring correctly the merging properties of galaxies.

This paper is organised as follows: §2 includes a discussion of the data sources we use in this paper, and how we select our sample, including a description of our morphological and structural analyses, and the stellar masses we utilise, §3 is a discussion of our results, including a description of the merger history up to $z \sim 1.2$, and §4 is our summary and conclusions. We use a standard cosmology of $H_0 = 70 \text{ km s}^{-1} \text{ Mpc}^{-1}$, and $\Omega_m = 1 - \Omega_\Lambda = 0.3$ throughout.

2 DATA AND SAMPLE SELECTION

2.1 Data

The data we use in the paper originate from the Extended Groth Strip (EGS) survey (Davis et al. 2007), and the COSMOS survey (Scoville et al. 2007). The selection of galaxies which we analyse is simply those systems which have a stellar mass $M_* > 10^{10} M_\odot$. As the EGS and the COSMOS fields have different data sets, and methods for galaxy detection, and for measuring stellar masses, we consider both data sets separately in what follows. In total there are 21,902 $M_* > 10^{10} M_\odot$ galaxies at $z < 1.2$ in our sample, with 2,388 galaxies in the EGS and 19,514 in the COSMOS field.

The main data set for this paper is the COSMOS field, which is by far the largest mosaic of Hubble Space Telescope imaging using the Advanced Camera for Surveys (ACS). The COSMOS ACS coverage is 1.8 deg^2 and is imaged in the F814W (I) band over this entire area with 1 orbit depth per pointing, for a total of 590 orbits. The 50% completeness of the COSMOS ACS data is $I_{AB} = 26$ (Scoville et al. 2007). The COSMOS field also has extensive optical data, described in Mobasher et al. (2007), from which stellar masses and photometric redshifts are computed. The photometric data in which these quantities are derived include optical data in the u^* band from the CFHT, $BgVriz$ imaging from the SuprimeCam on Subaru, i^- imaging from CFHT and K_S imaging from FLAMINGOS taken at CTIO and Kitt Peak (Mobasher et al. 2007). The I_{814} ACS imaging is also included in the analysis. The seeing for this optical

and NIR ground based imaging is roughly $1''$, with depths that range from 21.5 AB in K_s to ~ 27 in the r -band. The depth in every band is in any case well matched to image the most massive galaxies at $z < 1.2$ at a high S/N.

The ACS imaging of the EGS field covers a $10.1' \times 70.5'$ strip, for a total area of 0.2 deg^2 . This ACS imaging is discussed in Lotz et al. (2008) and Conselice et al. (2008b), and is briefly described here. The imaging consists of 63 tiles imaged in both the F606W (V) and F814W (I) bands. The $5\text{-}\sigma$ depths reached in these images are $V = 26.23$ (AB) and $I = 27.52$ (AB) for point sources, and about two magnitudes brighter for extended objects.

Our sample for the EGS comes from those systems which have K-band data taken as part of the Palomar Observatory Wide-field Infrared Survey (POWIR; Bundy et al. 2006; Conselice et al. 2007a,b; 2008b). The POWIR survey was designed to obtain deep K-band and J-band data over a significant ($\sim 1.5 \text{ deg}^2$) area. Observations were carried out between September 2002 and October 2005 over a total of ~ 70 nights. This survey covers the GOODS field North (Gialavalisco et al. 2004; Bundy et al. 2005), the Extended Groth Strip (Davis et al. 2007), and three other fields that the DEEP2 team has observed with the DEIMOS spectrograph (Davis et al. 2003). The total area we cover in the K-band is $5524 \text{ arcmin}^2 = 1.53 \text{ deg}^2$, with half of this area imaged in the J-band. Each of our fields reach $5\text{-}\sigma$ depths between $K_{s,\text{vega}} = 20.5 - 21.5$ for point sources, as measured in a $2''$ diameter aperture with the EGS.

Our K_s -band data were acquired utilising the WIRC camera on the Palomar 5 meter telescope. WIRC has an effective field of view of $8.1' \times 8.1'$, with a pixel scale of $0.25'' \text{ pixel}^{-1}$. Our K_s -band data were taken using 30 second integrations, with four exposures per pointing, while the J-band observations were taken with 120 second exposures per pointing. Typical total exposure times are one and two hours for both bands. Our reduction procedure follows standard methods for combining NIR ground-based imaging, and is described in more detail in Bundy et al. (2006). The resulting seeing FWHM in the K_s -band imaging ranges from $0.8''$ to $1.2''$, and is typically $1.0''$ (e.g., Bundy et al. 2006). Other data sets within the EGS we use consist of: optical imaging from the CFHT over all fields, imaging from the Advanced Camera for Surveys (ACS) on Hubble, and spectroscopy from the DEIMOS spectrograph on the Keck II telescope (Davis et al. 2003). A summary of these ancillary data sets are included in Davis et al. (2007) and Conselice et al. (2007b).

The optical imaging of the EGS is taken with the CFHT 3.6-m telescope. This optical data consists of imaging in the B, R and I bands taken with the CFH12K camera - a $12,288 \times 8,192$ pixel CCD mosaic with a pixel scale of $0.21''$. The integration times for these observations are 1 hour in B and R, and 2 hours in I, per pointing, with a R-band $5\text{-}\sigma$ depth of $R_{AB} \sim 25.1$, and similar depths at B and I. The seeing for the optical imaging is roughly the same as that for the NIR imaging, and we measure photometry using a $2''$ diameter aperture.

2.2 Redshifts

We utilise both spectroscopic and photometric redshifts for the galaxies we study in both the EGS and COSMOS fields.

The only field which has extensive available spectroscopy is the EGS. EGS Keck spectra were acquired with the DEIMOS spectrograph as part of the DEEP2 redshift survey (Davis et al. 2003). Target selection for the DEEP2 spectroscopy was based on the optical properties of the galaxies detected in the CFHT photometry, with the basic selection criteria $R_{AB} < 24.1$. DEEP2 spectroscopy was acquired through this magnitude limit, with no strong colour cuts applied to the selection. About 10,000 redshifts are measured for galaxies within the EGS. The sampling rate for galaxies that meet the selection criteria is 60%.

This DEIMOS spectroscopy was obtained using the 1200 line/mm grating, with a resolution $R \sim 5000$ covering the wavelength range 6500 - 9100 Å. Redshifts were measured through an automatic method comparing templates to data, and we only utilise those redshifts measured when two or more lines were identified, providing very secure measurements. Roughly 70% of all targeted objects result in secure redshifts.

As the COSMOS field is the major contributor to the data used in this paper we give a description of the photometric redshifts which we utilise. The details of its photometric redshifts and the catalog we use is described in great detail in Mobasher et al. (2007). We give a short summary here. The COSMOS photometric redshifts are measured through a standard template fitting technique. The templates used by Mobasher et al. (2007) are galaxies of various spectral types from ellipticals to starbursts across optical rest-frame wavelengths. The photometric redshifts we use were tested by comparing with 868 spectroscopic redshifts from the zCOSMOS survey, where the rms scatter in the agreement between photometric redshifts and spectroscopic redshifts is $\sigma(\Delta(z)) = 0.031$, where $\Delta(z) = (z_{\text{phot}} - z_{\text{spec}})/(1 + z_{\text{spec}})$ (Mobasher et al. 2007). Less than 2.5% of the galaxies are outliers in the agreement between spectroscopic and photometric redshifts. Mobasher et al. (2007) furthermore test their method of measuring photometric redshifts by calculating values using three different codes, and find a good agreement with their own calculation.

We utilise our own photometric redshifts within the EGS (e.g., Bundy et al. 2006; Conselice et al. 2007b, 2008b). The determination of the EGS photometric redshifts is done in a different way than in the COSMOS field. Within the EGS, photometric redshifts are based on the optical+near infrared imaging, in the BRIJK bands, and are fit in two ways, depending on the brightness of a galaxy in the optical. For galaxies that meet the spectroscopic criteria, $R_{AB} < 24.1$, we utilise a neural network photometric redshift technique to take advantage of the vast number of secure redshifts with similar photometric data. Most of the $R_{AB} < 24.1$ sources not targeted for spectroscopy should be within our redshift range of interest, at $z < 1.4$.

The neural network fitting is done through the use of the ANNz (Collister & Lahav 2004) method and code. To train the code, we use the ~ 5000 redshifts in the EGS, which has galaxies spanning our entire redshift range. The training of the photometric redshift fitting was in fact only done using the EGS field, whose galaxies are nearly completely selected based on a magnitude limit of $R_{AB} < 24.1$. We then use this training to calculate the photometric redshifts for galaxies with $R_{AB} < 24.1$. The agreement between our photometric redshifts and our ANNz spectroscopic redshifts is very good

using this technique, with $\delta z/(1+z) = 0.07$ out to $z \sim 1.4$. The agreement is even better for the $M_* > 10^{11} M_\odot$ galaxies where we find $\delta z/(1+z) = 0.025$ across all of our four fields (Conselice et al. 2007b).

For galaxies which are fainter than $R_{AB} = 24.1$ in the EGS we utilise photometric redshifts using Bayesian techniques, and the software from Benitez (2000). For an object to have a photometric redshift we require that it be detected at the 3σ level in all optical and near-infrared (BRIJK) bands, which in the R-band reaches $R_{AB} \sim 25.1$. We optimised our results, and correct for systematics, through the comparison with spectroscopic redshifts, resulting in a redshift accuracy of $\delta z/z = 0.17$ for $R_{AB} > 24.1$ systems. These $R_{AB} > 24.1$ galaxies are, however, only a very small part of our sample. Furthermore, all of these systems are at $z > 1$.

2.3 Stellar Masses

Since stellar masses are a critical aspect of this analysis, we go into some detail for how these are calculated. The stellar masses for the COSMOS survey are taken from Mobasher et al. (2007). These stellar masses are computed through the use of K-band imaging and the measured rest-frame $(B-V)_0$ colours of galaxies within COSMOS. Mobasher et al. (2007) use this measured colour to obtain a mass to light ratio through the relation:

$$M/L_v = -0.628 + 1.305(B - V)_0 \quad (1)$$

which assumes a Salpeter IMF within a mass range of $0.1 M_\odot$ to $100 M_\odot$. The colours used in this analysis are not directly measured from the data, but are taken from the best fit templates of various types (E, Sa, Sb, Sc, Im and starburst) (see Mobasher et al. 2007). Due to limited K-band data over the COSMOS field, the stellar masses of these galaxies are calculated via rest-frame V-band magnitudes with the equation:

$$\log(M_{\text{stellar}}/M_\odot) = M/L_V - 0.4 * (M_V - 4.82). \quad (2)$$

Mobasher et al. (2007) discuss using V-band luminosities for measuring stellar masses rather than K-band, which is very shallow over the COSMOS fields. They find for a subset of their sources, which are detected in the K-band, an agreement with the V-band based stellar masses, these are however the reddest, and thus perhaps the most evolved galaxies, and therefore may not be representative.

Within the EGS field we match our K-band selected catalogs to the CFHT optical data to obtain spectral energy distributions (SEDs) for all of our sources, resulting in measured BRIJK magnitudes. From these we compute stellar masses based on the methods and results outlined in Bundy, Ellis, Conselice (2005) and Bundy et al. (2006). All our stellar masses are furthermore normalised by the observed rest-frame K-band light, which is roughly at rest-frame $\sim 1 \mu m$, or redder, for most galaxies. We also convert these stellar masses, which are calculated in equation (2) using a Salpeter IMF to a Chabrier IMF.

The basic mass fitting method within the EGS consists of fitting a grid of model SEDs constructed from Bruzual & Charlot (2003) (BC03) stellar population synthesis models, with different star formation histories. We use an exponentially declining model to characterise the star formation

history, with various ages, metallicities and dust contents included. These models are parameterised by an age, and an e-folding time for parameterising the star formation history, where $\text{SFR} \sim e^{-t/\tau}$. The values of τ are randomly selected from a range between 0.01 and 10 Gyr, while the age of the onset of star formation ranges from 0 to 10 Gyr. The metallicity ranges from 0.0001 to 0.05 (BC03), and the dust content is parametrised by τ_v , the effective V-band optical depth for which we use values $\tau_v = 0.0, 0.5, 1, 2$. Although we vary several parameters, the resulting stellar masses from our fits do not depend strongly on the various selection criteria used to characterise the age and the metallicity of the stellar population.

It is important to realise that these parameterisations are fairly simple, and it remains possible that stellar mass from older stars is missed under brighter, younger, populations. While the majority of our systems are passively evolving older stellar populations, it is possible that up to a factor of two in stellar mass is missed in any star bursting blue systems. However, stellar masses measured through our technique are roughly the expected factor of 5-10 smaller than dynamical masses at $z \sim 1$ using a sample of disk galaxies (Conselice et al. 2005b), demonstrating their inherent reliability.

We match magnitudes derived from these model star formation histories to the actual data to obtain a measurement of stellar mass using a Bayesian approach. We calculate the likely stellar mass, age, and absolute magnitudes for each galaxy at all star formation histories, and determine stellar masses based on this distribution. Distributions with larger ranges of stellar masses have larger resulting uncertainties. While parameters such as age, e-folding time, metallicity, etc. are not likely accurately fit through these calculations due to various degeneracies, the stellar mass is robust. Typical errors for our stellar masses are 0.2 dex from the width of the probability distributions. There are also uncertainties from the choice of the IMF. Our stellar masses utilise the Chabrier (2003) IMF. There are additional random uncertainties due to photometric errors. The resulting stellar masses thus have a total random error of 0.2-0.3 dex, roughly a factor of two.

Furthermore, there is the issue of whether or not our stellar masses are overestimated based on using the Bruzual & Charlot (2003) models. It has recently been argued by Maraston (2007), among others, that a refined treatment of thermal-pulsating AGB stars in the BC03 models result in stellar masses that can be too high by a factor of a few. While we consider an uncertainty of a factor of two in our stellar masses, it is worth investigating whether or not our sample is in the regime where the effects of a different treatment of TP-AGB stars in e.g., Maraston (2007) will influence our mass measurements. This has been investigated in Maraston (2005) who have concluded that galaxy stellar masses computed with an improved treatment of TP-AGB stars are roughly 50-60% lower.

However, the effect of TP-AGB stars is less important at our rest-frame wavelengths probed than at longer wavelengths, especially in the rest-frame IR. The EGS survey is K-selected, and the observed K-band is used as the flux in which stellar masses are computed. The rest-frame wavelength probed with the observed K-band ranges from $0.7 \mu m$ to $1.5 \mu m$ where the effects of TP-AGB stars are minimised.

The ages of our galaxies are also older than the ages where TP-AGB stars have their most effect (Maraston 2005). To test this, after our analysis was finished, we utilised the newer Bruzual and Charlot (2009, in prep) models, which include a new TP-AGB star prescription, on our massive galaxy sample. From this we find on average a ~ 0.07 dex smaller stellar mass using the newer models. At most, the influence of TP-AGB stars will decrease our stellar masses by 20%. The effect of this would decrease the number of galaxies within our sample, particularly those close to the $M_* = 10^{10} M_\odot$ boundary. This systematic error is however much smaller than both the stellar mass error we assume (0.3 dex), and the cosmic variance uncertainties, and thus we conclude it is not a significant factor for our analysis.

2.4 The Extended CAS Structural Analysis

We use the CAS (concentration, asymmetry, clumpiness) parameters to measure the structures of our $z < 1.2$ galaxies quantitatively. We include in our analysis the measurement of the Gini and M_{20} parameters (e.g., Lotz et al. 2008). The CAS/Gini/ M_{20} parameters are a non-parametric method for measuring the forms and structures of galaxies in resolved CCD images (e.g., Conselice et al. 2000a; Bershady et al. 2000; Conselice et al. 2002; Conselice 2003; Lotz et al. 2008). The basic idea behind these parameters is that galaxies have light distributions that reveal their past and present formation modes (Conselice 2003). Furthermore, well-known galaxy types in the nearby universe fall in well defined regions of the CAS parameter space. For example, the selection $A > 0.35$ locates systems which are nearly all major galaxy mergers in the nearby universe (e.g., Conselice et al. 2000b; Conselice 2003; Hernandez-Toledo et al. 2005; Conselice 2006b). In addition to the classic CAS parameters, we also investigate the use of the similar Gini and M_{20} parameters (Lotz et al. 2008). We give a brief description of these parameters below.

The way we measure structural parameters on our Hubble images varies slightly from what has been done earlier in the Hubble Deep Field, and GOODS imaging (e.g., Conselice et al. 2003a; Conselice et al. 2004). The basic measurement procedure, after cutting out the galaxy into a smaller image, is to first measure the radius in which the parameters are computed. The radius we use for all our indices is defined by the Petrosian radii, which is the radius where the surface brightness at a given radius is 20% of the surface brightness within that radius (e.g., Bershady et al. 2000; Conselice 2003).

We use circular apertures for our Petrosian radii and quantitative parameter estimation. We begin our estimates of the galaxy centre for the radius measurement at the centroid of the galaxy's light distribution. Through modelling and various tests, it can be shown that the resulting radii do not depend critically on the exact centre, although the CAS and other parameters do (Conselice et al. 2000; Lotz et al. 2004). The exact Petrosian radius we use to measure our parameters is

$$R_{\text{Petr}} = 1.5 \times r(\eta = 0.2),$$

where $r(\eta = 0.2)$ is the radius where the surface brightness is 20% of the surface brightness within that radius.

A very important issue, especially for faint galaxies, is how to account for background light and noise. For faint galaxies there is a considerable amount of noise added due to the sky, which must be corrected. Through various test, outlined in detail in Conselice et al. (2009, in prep), we conclude that the proper way to correct parameters for the background requires that the selected background area be close to the object of interest. This is only an issue for faint galaxies, and for galaxies imaged on large mosaics which have a non-uniform weight map, and whose noise characteristics vary across the field. By using a background near each object we alleviate these issues as the noise properties do not vary significantly over $\sim 0.5 - 1$ arcmin, where the galaxy and the background area are selected. We review below how the CAS and Gini/ M_{20} parameters are measured. For more detail see Bershady et al. (2000), Conselice et al. (2000), Conselice (2003), and Lotz et al. (2008).

2.4.1 Asymmetry

The asymmetry of a galaxy is measured by taking an original galaxy image and rotating it 180 degrees about its centre, and then subtracting the two images (Conselice 1997). There are corrections done for background, and radius (explained in detail in Conselice et al. 2000a). Most importantly, the centre for rotation is decided by an iterative process which finds the location of the minimum asymmetry. The formula for calculating the asymmetry is given by:

$$A = \min \left(\frac{|\Sigma I_0 - I_{180}|}{\Sigma I_0} \right) - \min \left(\frac{|\Sigma B_0 - B_{180}|}{\Sigma I_0} \right) \quad (3)$$

Where I_0 is the original image pixels, I_{180} is the image after rotating by 180° . The background subtraction using light from a blank sky area, called B_0 , are critical for this process, and must be minimised in the same way as the original galaxy itself. A lower value of A means that a galaxy has a higher degree of rotational symmetry which tends to be found in elliptical galaxies. Higher values of A indicate an asymmetric light distribution, which are usually found in spiral galaxies, or in the more extreme case, merger candidates.

2.4.2 Concentration

Concentration is a measure of the intensity of light contained within a central region in comparison to a larger region in the outer-parts of a galaxy. The exact definition is the ratio of two circular radii which contain 20% and 80% (r_{20} , r_{80}) of the total galaxy flux,

$$C = 5 \times \log \left(\frac{r_{80}}{r_{20}} \right). \quad (4)$$

This index is sometimes called C_{28} . A higher value of C indicates that a larger amount of light in a galaxy is contained within a central region. This particular measurement of the concentration correlates well with the mass and halo properties of galaxies in the nearby universe (e.g., Bershady et al. 2000; Conselice 2003).

2.4.3 Clumpiness

The clumpiness (S) parameter is used to describe the fraction of light in a galaxy which is contained in clumpy distributions. Clumpy galaxies have a relatively large amount of light at high spatial frequencies, whereas smooth systems, such as elliptical galaxies contain light at low spatial frequencies. Galaxies which are undergoing star formation tend to have very clumpy structures, and high S values. Clumpiness can be measured in a number of ways, the most common method used, as described in Conselice (2003) is,

$$S = 10 \times \left[\left(\frac{\Sigma(I_{x,y} - I_{x,y}^{\sigma})}{\Sigma I_{x,y}} \right) - \left(\frac{\Sigma(B_{x,y} - B_{x,y}^{\sigma})}{\Sigma I_{x,y}} \right) \right], \quad (5)$$

where, the original image $I_{x,y}$ is blurred to produce a secondary image, $I_{x,y}^{\sigma}$. This blurred image is then subtracted from the original image leaving a residual map, containing only high frequency structures in the galaxy (Conselice 2003). To quantify this, we normalise the summation of these residuals by the original galaxy's total light, and subtract from this the residual amount of sky after smoothing and subtracting it in the same way. The size of the smoothing kernel σ is determined by the radius of the galaxy, and is $\sigma = 0.2 \cdot 1.5 \times r(\eta = 0.2)$ (Conselice 2003). Note that the centres of galaxies are removed when this procedure is carried out.

2.4.4 Gini and M_{20} Coefficients

The Gini coefficient is a statistical tool originally used in economics to determine the distribution of wealth within a population, with higher values indicating a very unequal distribution (Gini of 1 would mean all wealth/light is in one person/pixel), while a lower value indicates it is distributed more evenly amongst the population (Gini of 0 would mean everyone/every pixel has an equal share). The value of G is defined by the Lorentz curve of the galaxy's light distribution, which does not take into consideration spatial position. Each pixel is ordered by its brightness and counted as part of the cumulative distribution (see Lotz et al. 2004, 2008).

The M_{20} parameter is a similar parameter to the concentration in that it gives a value that indicates whether light is concentrated within an image; it is however calculated slightly differently. The total moment of light is calculated by summing the flux of each pixel multiplied by the square of its distance from the centre. The centre is deemed to be the location where M_{20} is minimised (Lotz et al 2004). The value of M_{20} is the moment of the fluxes of the brightest 20% of light in a galaxy, which is then normalised by the total light moment for all pixels (Lotz et al. 2004, 2008).

3 ANALYSIS

3.1 Characteristics of the Sample

This analysis is unique in several ways. First, it is based on two major data sets - the COSMOS and the EGS surveys. The total number of galaxies we study for our morphological analysis is also by far the largest ever published to date. Similar previous work using the GOODS fields, the Hubble Deep Fields, and the Hubble Ultra Deep Field (e.g., Conselice et al. 2003; Conselice et al. 2003, 2004; Conselice et

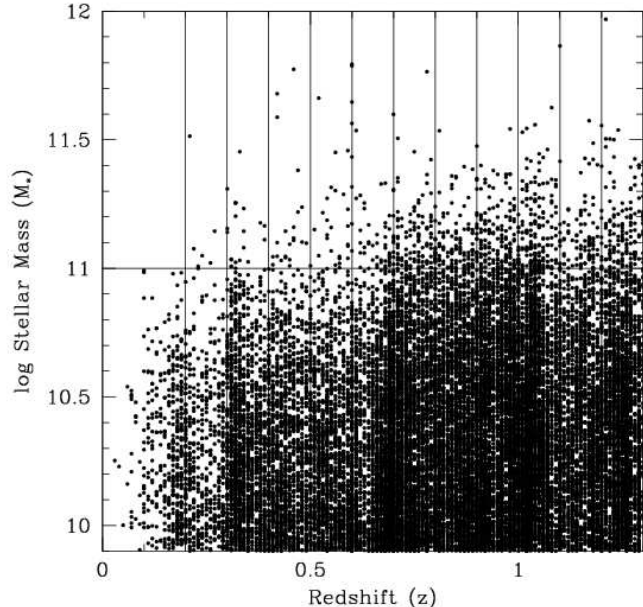


Figure 1. The stellar mass vs. redshift (z) relation for the COSMOS field. The vertical lines show the redshift limits for the various bins we use within our analysis. The horizontal line represents the cut at $\log M_* = 11$ we use in some of our analysis. Note that the clustered redshift peaks are due to real over-densities. The distribution within the EGS for the same stellar mass range is similar (Conselice et al. 2007a).

al. 2005; Lotz et al. 2008) used smaller samples, and thus were able to check systematics in a way we cannot due to our large sample of galaxies. The large number of galaxies in our sample makes the type of checking done in previous work largely impossible (cf. Jogee et al. 2008 for this type of analysis done on the GEMS data set).

The sample of galaxies in which we use from the EGS is described in great detail in Conselice et al. (2007b), and we refer all readers to this paper for characteristics of the sample. The sample we use for the COSMOS field is however not as well characterised, nor as well understood, or as accurately calibrated. We can however, investigate some basic features of the COSMOS data set to determine how it compares with the better calibrated (for our purposes) EGS data set and sample, described in Conselice et al. (2007b).

Figure 1 shows how stellar masses are distributed with redshift in the COSMOS field, demonstrating some clustering features which may bias the results, if the merger history is a strong function of environment. The COSMOS field is known to contain a mixture of environments from single galaxies to large groups (Scoville et al. 2007), and our sample is taken from all of these environments.

The other feature through which we investigate the sample is the CAS diagrams of concentration-asymmetry and asymmetry-clumpiness (Conselice 2003). These diagrams reveal which type of galaxies are likely to be within the sample. What we found in our initial analysis is that a significant number of systems within the COSMOS field had concentration values near $C = 2$, which is typically found for stars. Visual inspection of these images reveals that this

is indeed the case - many stars appear to be within the released COSMOS galaxy catalogs. On the other hand, our star/galaxy separation in the EGS (see Conselice et al. 2007 and references therein) was very effective at removing stars and no such contamination is found in the $C - A$ diagrams. We utilize the fact that stars have a well defined concentration and small measured radii to remove these systems from our COSMOS CAS catalog.

Figure 2 shows the resulting concentration-asymmetry diagram at $z > 0.75$ and $z < 0.75$ for the combined COSMOS and EGS sample. What this reveals is that there is a wide diversity of structures for galaxies at all redshifts, as shown using smaller samples in e.g., Conselice et al. (2003, 2005) and Lotz et al. (2008). This includes galaxies which would be classified at $z = 0$ as early types, late-types, and systems which are asymmetric enough to be ongoing major mergers (Conselice 2006a).

One of the most interesting things concerning Figure 2 is the clear bimodality of the structural parameters for these systems. At both redshifts bins, there is a peak in the density contours near the mid/early-type range, and another peak well within the late-type range. This bimodality is present within all redshifts, and is the same bimodality found using similar structural parameters by Zamojski et al. (2007) within COSMOS. At $z < 0.75$ we find one peak at $C = 3.9$ and $A = 0.1$, and the other peak at $C = 2.9$ and $A = 0.2$. These two values of C and A are equivalent to early-types and late-type galaxies, and is likely similar to the bimodality found within the colour-magnitude diagram (e.g., the red-sequence and blue cloud).

Another interesting feature of Figure 2 is that the peak location for the centres of the bimodality differs slightly with redshift, becoming less concentrated and more asymmetric at high redshift. This change is $\delta A = 0.05$ and $\delta C = 0.2$. The peaks of the bimodality are also softer, suggesting a larger scatter about the bimodality seen at lower redshifts. The slightly lower values are in principle due solely to redshift effects, or morphological k-corrections, both of which are roughly of the order of the changes seen here.

3.2 Selection of Mergers

Before we can effectively study the merger history for our sample, we must select a robust sample of mergers, as cleanly as possible (e.g., Conselice et al. 2008a). There are several ways to do this. The classical rest-frame optical CAS definition for determining whether a system is undergoing a merger is given by (Conselice 2003):

$$A > 0.35 \text{ and } A > S, \quad (6)$$

That is, the asymmetry A must be larger than 0.35 and the asymmetry must exceed the value of the clumpiness of the galaxy. This selection will nearly always cleanly find galaxies in mergers as revealed through nearby samples of galaxies (Conselice 2003; De Propriis et al. 2007), and through N-body simulations of the merger process (Conselice 2006). Tests of how well this criteria does at higher redshifts are limited to either small samples (Conselice et al. 2008a), and to the GEMS survey which was based on F606W (V) band imaging of galaxies (Jogee et al. 2008). These studies however reveal a few features that we can use to determine how

well the criteria given in equation (6) does for finding galaxies undergoing mergers.

The first is that although the Jogee et al. (2008) study of GEMS uses the F606W band, at $z = 0.4$, it samples rest-frame optical light, as we also do for nearly all our galaxy sample. Since Jogee et al. (2008) classify all their galaxies by eye (which we do not), and use the exact same methodology and CAS code as we do, we can use their analysis to determine what fraction of galaxies we are finding using criteria from eq. (6) which are actual merging galaxies. Jogee et al. (2008) find that at their lowest redshift, the contamination by non-merging galaxies, as defined by visual inspection, is $\sim 30\%$. A significant fraction of this 30% however are irregular galaxies, some of which could be systems in some phase of a merger. Conselice et al. (2008a) within the UDF, found that over the entire redshift range of $0.4 < z < 3$ the contamination is lower, roughly 15%. These differences are likely due to the difficulty of defining what a merger is based on visual appearances.

We also use the clumpiness-asymmetry diagrams of our combined sample and the concentration-asymmetry diagram discussed in §3.1 to get an idea for how well the merger criteria selects merging systems. First, we note that in Paper I (Conselice et al. 2008a) the clumpiness-asymmetry relation found for normal galaxies in Conselice (2003) does not do a good job in tracing the relation between asymmetry and clumpiness for normal, non-merging, galaxies. For systems at $z > 0.4$ the clumpiness values are lower than their corresponding asymmetry. This is due to either to the structures of galaxies being actually less clumpy, or in the way the clumpiness is defined by Conselice (2003), or because of decreased resolution and S/N, the clumpiness decreases.

We reevaluate the criteria for how the asymmetry and clumpiness values for normal galaxies change for galaxies at $z > 0.4$ through the use of the Hubble Ultra Deep Field (described in Paper I). The relation between S and A for all galaxies in the Conselice et al. (2008a) sample is shown in Figure 3. The solid line in Figure 3 is the best fit relation between the asymmetry and clumpiness indices for the normal galaxies - i.e., those that are not merging or peculiar at $z > 0.2$. This relation is given by

$$A = (0.99 \pm 0.14) \times S + (0.05 \pm 0.01), \quad (7)$$

which is roughly $A \sim S$. In Figure 4 we show the relation between A and S for the COSMOS+EGS sample. As can be seen, there is a general correlation between these two parameters, with a single peak, and a distribution around $S = 0.1$ and $A = 0.15$. Figure 4 also shows that the average asymmetry of these galaxies slightly increases at higher redshifts, with the clumpiness index remaining roughly the same at the peak value.

3.3 The Merger Fraction

3.3.1 Merger Fractions

Understanding the merger history of galaxies is important for deriving how the merger process drives the assembly of galaxies, as well as its possible role in the triggering of star formation and AGN activity. The merger fraction history at $z > 0.2$ is however considered somewhat controversial, due to published values of the derived merger history differing

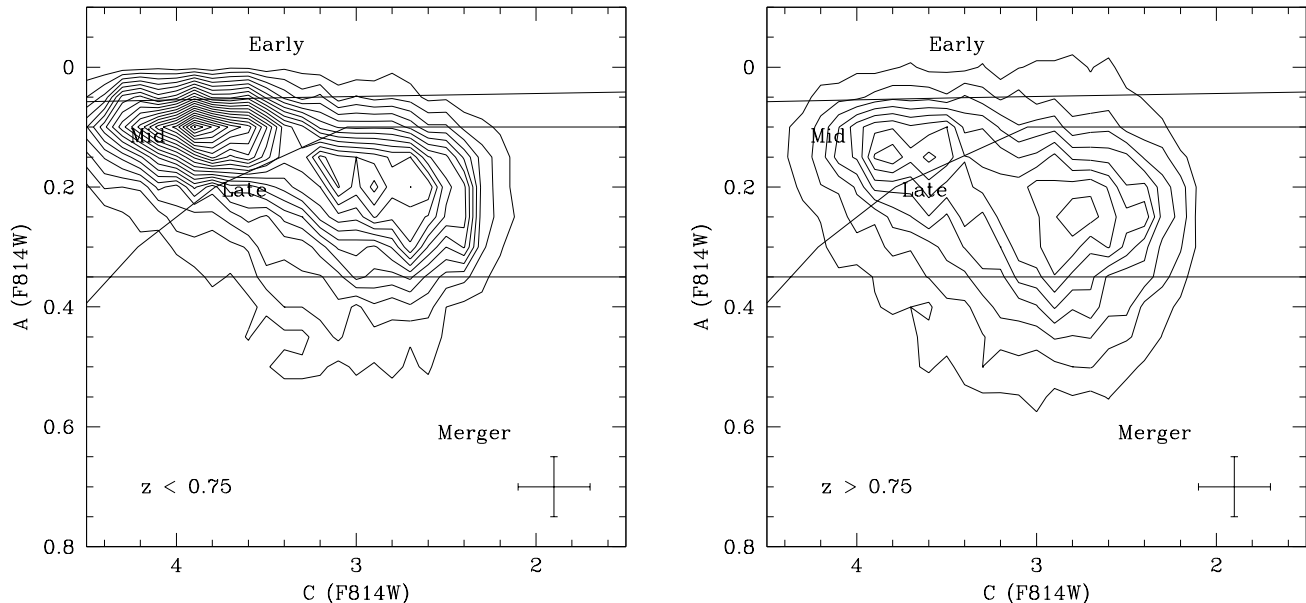


Figure 2. The relationship between the asymmetry (A) and the concentration (C) for galaxies within the combined EGS+COSMOS sample we examine in this paper. Due to the large number of points we have used contours to examine this distribution. The solid lines denote regions for galaxies of different types which are labelled within their respective regions. In general, galaxies which are at $A > 0.35$ are those which are found to be ongoing major mergers. We divide our sample into two roughly equivalent sample sizes, with the galaxies at $z < 0.75$ shown on the left and those at $z > 0.75$ plotted on the right. As can be seen, and discussed within the paper, each redshift bin displays a bimodality in the galaxy population. The higher redshift bins shows peaks in this bimodality that are slightly offset from the lower redshift bin, but the galaxies at $z > 0.75$ also show a large distribution of points, with the peaks not as well defined.

(e.g., Conselice et al. 2003a; Lotz et al. 2008; de Ravel et al. 2008). In this section we examine the merger history for massive galaxies ($M_* > 10^{10} M_\odot$) using our combined EGS and COSMOS data sets.

One of the benefits of using the CAS system for finding mergers is that it allows us to quantify the merger fraction, merger rates, and thus the number of mergers occurring in a galaxy population (Conselice et al. 2003a; Conselice 2006b). The reason for this is that the CAS method has been well calibrated in terms of the types of galaxies picked up with various selection criteria at different redshifts, as well as estimates for the time-scale sensitivity and the ability to pick up mergers with different mass ratios. In this section we investigate the merger fractions based on standard techniques we have developed (e.g., Conselice 2003; Conselice 2006; Bridge et al. 2007; §3.2).

There are a few caveats to measuring the merger fraction which we must consider before using these values to determine how galaxies are evolving due to major mergers, and to measure the merger fraction at any redshift. We discuss these issues in §3.3.2. We determine the final correction for asymmetries based on redshift and contamination effects, and use these to calculate the merger fraction evolution at $z < 1.2$, which we discuss in §3.3.3. In §3.3.4 we use these merger fractions to parameterise the merger history. We use these results in later subsections of §3 to determine the merger rate, and the average number of mergers galaxies of various masses undergo at different redshifts.

3.3.2 Redshift Effects and Contamination

The basic merger fraction (f_m) is calculated as the number of mergers selected within a given redshift bin and stellar mass limit (N_m), divided by the total number of galaxies within the same redshift and stellar mass bin (N_T),

$$f_m(M_*, z) = \frac{N_m}{N_T}. \quad (8)$$

However, there are several issues that have to be considered before we can use equation (8) to derive the merger fraction. One factor we have to account for are the effects of redshift on the measured CAS parameters of our galaxies. These effects include the lowering of surface brightness, and morphological k -corrections, on the measurement of merger fractions using the COSMOS and the EGS data. We address these two corrections separately and quantitatively. We also discuss how to account for the contamination rate due to non-mergers within our sample.

Some of these issues were addressed, at least in terms of redshift effects, by Kampczyk et al. (2007) who examined how a volume limited sample of 1813 low redshift galaxies in the Sloan Digital Sky Survey would appear at higher redshifts in the COSMOS field. Kampczyk et al. (2007) simulated galaxy mergers at low redshift to how they would appear at high redshift within COSMOS. They also investigated what fraction of normal galaxies would be misidentified as mergers due to chance superpositions, and other effects. They found that only one in five of the merging galaxies in the SDSS would still be identified as such if placed

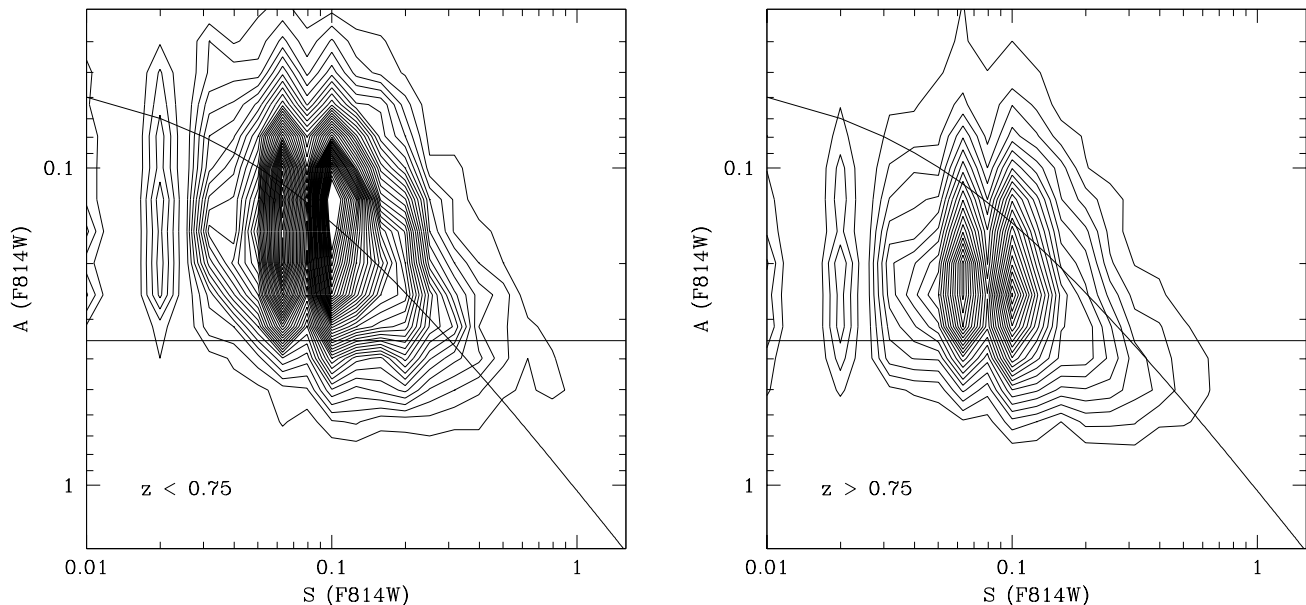


Figure 4. The relationship between the asymmetry (A) and the clumpiness (S) indices for galaxies within our combined EGS+COSMOS sample. The galaxies in this figure and the division between redshifts is the same as in Figure 2. The horizontal solid line shows the $A = 0.35$ limit for finding mergers, and the curved solid line shows the relation between A and S for normal galaxies at $z < 1.2$ as found in the UDF and plotted in Figure 3.

at $z \sim 1$, after imaged within COSMOS. Kampczyk et al. (2007) also found that 1.7% of normal SDSS galaxies would be identified as mergers due to chance superpositions. They however conclude that most of the mergers they identify by eye in COSMOS at $z \sim 1$ are real.

We go beyond Kampczyk in this paper in a number of ways. First we use quantitative methods that do not rely upon subjective understanding of what a merger is. Because we purely use the CAS system in this paper, our approach is quantitative and repeatable, and not subject to classification bias. We also quantify directly using simulations how much the parameters we measure are affected by redshift effects, not just the effects of signal to noise and resolution examined by Kampczyk et al. (2007). We also note that Kampczyk et al. (2007) find that the mergers they simulate remain asymmetric, but that the Gini/ M_{20} method fails to locate 90% of their merging galaxies, similar to our findings in the Hubble Ultra Deep Field (Paper I; Conselice et al. 2008a).

Since we use the F814W data to measure the CAS values, and therefore merger fractions, of our galaxies, we are sampling different rest-frame wavelengths for galaxies at different redshifts. We address this empirically in two different ways. The first is that we can use imaging from the Hubble Ultra Deep Field, where we have BViz imaging for all galaxies, to determine the morphological k -correction present within our galaxies, as discussed in Conselice et al. (2008a). The other is that we can use the F606W (V-band) and F814W (I-band) data from the EGS as another determi-

nation for how the morphological k -correction changes the resulting measured CAS parameters.

The F814W band at observed $\lambda = 8332 \text{ \AA}$ results in a range of probed rest-frame wavelengths from $0.7 \mu\text{m}$ at $z = 0.2$, to $0.38 \mu\text{m}$ at $z \sim 1.2$. This spans roughly the entire optical wavelength range, where the CAS parameters can slight change (e.g., Conselice et al. 2000a). However, these resulting changes are not large (e.g., Taylor-Mager et al. 2007; Conselice et al. 2008a). As such, we investigate the changes using galaxies in the UDF, to determine how much the measured asymmetry in the F814W band changes due to the rest-frame wavelength probed.

We base our measurement of the morphological k -correction on how the measured CAS parameters, particularly the asymmetry index, change with respect to $\lambda = 5500 \text{ \AA}$. For systems at $z < 0.8$ we utilise the results of Conselice et al. (2008a) who find a change of asymmetry parameter with rest-frame wavelength in the optical of $\delta A_{k\text{-corr}}/\lambda = -0.30 \mu\text{m}^{-1}$ at $z < 0.75$. For galaxies at $z > 0.75$ Conselice et al. (2008a) find a change of $\delta A_{k\text{-corr}}/\lambda = -0.8 \mu\text{m}^{-1}$. The effective result of this is a maximum change in the asymmetry index of $\delta A_{k\text{-corr}} = 0.1$ at the highest redshifts. We perform this correction for each of our galaxies, such that we are measuring the CAS parameter at the same wavelength, in this case at rest-frame $\lambda = 5500 \text{ \AA}$. We find similar results when comparing the V and I band CAS values within the ACS imaging of the EGS.

Another correction due to redshift is the fact that the surface brightness declines with $(1+z)^4$, and thus the galax-

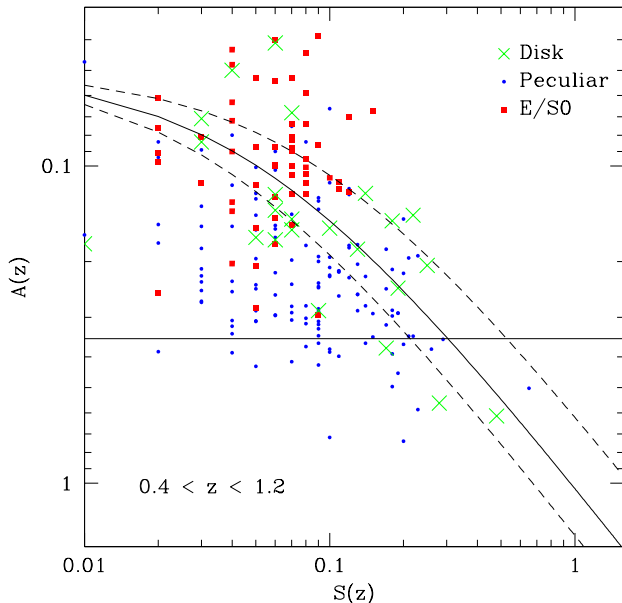


Figure 3. The relation between asymmetry and clumpiness for galaxies in the Hubble Ultra-Deep Field at $0.4 < z < 1.2$ from paper I (Conselice et al. 2008a). Shown are the three main types of galaxies classified within the UDF (ellipticals, disks and peculiars). The solid line shows the best fit relation between the A and the S parameters for the normal galaxies (disks and ellipticals). The dashed line shows the $3\text{-}\sigma$ deviation for this fit. As can be seen, the disk galaxies which have an asymmetry $A > 0.35$ generally follow this relation and have a relatively high asymmetry value for their clumpiness.

ies we image at $z \sim 1$, with the same effective surface brightness, will appear a factor of ~ 8 fainter in their measured surface brightness than at $z \sim 0.2$. We correct for this effect through simulations, as described previously in Conselice (2003) and Conselice et al. (2003a). These simulations involve nearby galaxies which are simulated to various redshifts, and their CAS parameters are measured and compared with those at lower redshifts. What we find is that up to $z \sim 1$, the CAS parameters are not affected to a large degree, and the asymmetry index declines by $\delta A_{\text{SB-dim}} \sim 0.05$ up to $z \sim 1$. We therefore use this as the maximum correction at $z \sim 1$ and apply it to galaxies at $z > 0.5$ where this effect is found to be important.

The other correction we perform is to correct the CAS merger fraction measures for contamination from galaxies which are within the merger region of CAS space, but which are not structurally undergoing a merger (see also §3.2 & Conselice et al. 2008a). The estimates of this correction must be done by eye, and the large sample in this paper makes this exercise too prohibitively large to carry out. Previous studies however have revealed what this fraction is from samples of ~ 1000 s of galaxies (Jogee et al. 2008; Conselice et al. 2008a). Conselice et al. (2008a) find that the contamination rate is roughly $14 \pm 10\%$ for galaxies observed in the z -band

(Conselice et al. 2008a). Other results include an examination of the CAS and morphological types for ~ 3600 galaxies in the GEMS V_{606} band (Jogee et al. 2008), which find a contamination rate of $f_{\text{contam}} \sim 30\%$ at $z = 0.3$ which is rest-frame $\sim 4500 \text{ \AA}$. Since the GEMS survey better matches the depth and rest-frame wavelength of our images, we use a contamination correction of $f_{\text{contam}} = 25\%$. This correction is potentially smaller than this due to the removal of ‘irregular’ galaxies from Jogee et al. (2008), some of which are potentially merging systems.

The final measure of the asymmetry index to calculate the merger fraction is given by:

$$A_{\text{final}} = (A_{\text{obs}} + \delta A_{\text{SB-dim}} + \delta A_{\text{k-corr}}) \times (1 - f_{\text{contam}}), \quad (9)$$

where $\delta A_{\text{k-corr}}$ is the (usually negative) morphological k-correction, $\delta A_{\text{SB-dim}}$ is the (positive) correction for redshift effects, and f_{contam} is the fraction of galaxies found through CAS which are not actually merging systems, which we take as $f_{\text{contam}} = 0.25$ in this paper.

3.3.3 The Merger Fraction Evolution

The first observation we derive from our CAS values is the evolution of the merger fraction (Figure 5) for both the EGS and COSMOS fields separately. Error bars reflect uncertainties due to shot noise, and photometric redshift errors. Before we discuss the merger fraction evolution it is important to address the issue of whether our merger analysis, which finds galaxies with a high asymmetry, locates the same types of galaxies at different redshifts. A legitimate concern is that at higher redshifts, galaxies can be asymmetric due to reasons other than major mergers, such as star formation and minor mergers.

Certainly, we know there are differences between galaxies at various redshifts, as for example, the star formation rate at $z = 1$ is several times higher than it is at $z = 0$. However, several detailed analyses over the past few years have shown that galaxies with high asymmetries are almost always major mergers. This includes calibrating how the asymmetry index works, not just at low redshifts (Conselice 2003), but also at high redshift (e.g., Conselice et al. 2005, 2008a). These studies have found that galaxies with evidence for merging, both kinematically (e.g., Kassin et al. 2007), and through visual inspection, have high asymmetries, and likewise the non-mergers are not asymmetric. Note that this is only true in optical light, as asymmetries for star forming galaxies in the rest-frame UV can be quite high, independent of any merging activity (Taylor-Mager et al. 2007).

It is also possible that interactions and minor mergers can produce large asymmetries. However, for reasons explained in previous papers, such as Conselice (2006b) and de Propriis et al. (2007), it is unlikely that very many asymmetric galaxies are produced through interactions or minor mergers. de Propriis et al. (2007) examined the asymmetry values for interacting, merging, and normal galaxies in the nearby universe. They found that very few of the interacting galaxies are considered mergers in the CAS system, and those that would be counted are in very close pairs which are about to merge. By far the bulk of the systems with high asymmetries are found in the major merger category. This was furthermore quantified through N-body simulations by Conselice (2006) who found that only major mergers with

Table 1. Merger Fractions for Galaxies with $M_* > 10^{10} M_\odot$

| z | f(EGS) | F(COSMOS) | F(EGS+COSMOS) |
|------|-----------------|-----------------|-----------------|
| 0.25 | ... | 0.05 ± 0.01 | 0.04 ± 0.01 |
| 0.35 | ... | 0.04 ± 0.01 | 0.04 ± 0.01 |
| 0.45 | 0.02 ± 0.02 | 0.04 ± 0.01 | 0.04 ± 0.01 |
| 0.55 | 0.04 ± 0.02 | 0.05 ± 0.01 | 0.04 ± 0.01 |
| 0.65 | 0.09 ± 0.03 | 0.11 ± 0.01 | 0.09 ± 0.01 |
| 0.75 | 0.11 ± 0.02 | 0.10 ± 0.01 | 0.12 ± 0.01 |
| 0.85 | 0.08 ± 0.02 | 0.12 ± 0.01 | 0.11 ± 0.01 |
| 0.95 | 0.09 ± 0.02 | 0.10 ± 0.01 | 0.10 ± 0.01 |
| 1.05 | 0.15 ± 0.02 | 0.11 ± 0.01 | 0.11 ± 0.01 |
| 1.15 | 0.15 ± 0.03 | 0.12 ± 0.01 | 0.13 ± 0.01 |

ratios of $> 1 : 4$ would be counted as a major merger within the CAS system. Because the asymmetry index, and the other CAS values, are luminosity weight, faint features, such as tidal debris (e.g. Kawata et al. 2006) do not produce large asymmetries.

We thus determine the merger fraction for galaxies of various masses using the criteria from equation (6) and by using the asymmetries calculated in equation (9). Our final merger fraction values are tabulated in Table 1, and are separated into the EGS and COSMOS fields in Figure 5. Figure 6 shows the merger fraction evolution for our $M_* > 10^{10} M_\odot$ sample, with the $z = 0.05$ point from De Propriis et al. (2007), and the $z > 1.2$ merger fractions from Conselice et al. (2008a).

We note that the merger fractions we measure are in no sense the total galaxy merger fraction, that is the total number of galaxies which have undergone, or are undergoing, a merger at the given time. Most galaxies will have undergone a merger sometimes in their history, and the fraction of galaxies which have undergone a merger sometime in the past will be close to 100%.

All merger fractions we derive in this paper are computed using the CAS parameters, which is only sensitive to a well defined time-range during the major merger process (Conselice 2006; Lotz et al. 2008b). In the case of CAS mergers, this time-span is roughly 0.4-1 Gyr (Conselice 2006; Lotz et al. 2008b). As shown in Conselice (2006) there are phases of a merger which will not be picked up by the CAS technique. A different technique will find a different merger fraction if it has a time sensitivity different from the CAS system. For example if galaxy pair methods has roughly a factor of two longer time-scale for finding a merger than the CAS system, the resulting computed merger rate would be the same, as the pair method would find a factor of two more galaxies merging than the CAS parameters. We therefore expect, and find there to be, galaxies that by eye appear as a merger, but do not have a high asymmetry (e.g., Conselice et al. 2008a).

There are a few obvious features of the merger fraction that deserve note, as seen in Figure 5 and 6. The first is that at the redshifts where we have data for both the EGS and COSMOS, the two agree remarkably well, always within $1-\sigma$ (see also Table 1). There is also a general trend for the merger fractions, as measured in both fields, to decline at

lower redshifts, going from $f_m = 0.15 \pm 0.03$ at $z = 1.2$ down to $f_m = 0.02 \pm 0.02$ at $z = 0.4$ in the EGS field, with a similar trend within the COSMOS field. The lowest redshift point for the COSMOS data at $z = 0.2$ is slightly higher than the two nearest and higher redshift bins. This is at least partially due to the higher resolution reached at this redshift, which can result in higher computed asymmetries (e.g., Conselice et al. 2000a).

The other obvious and outstanding feature of our measured merger history is the fact that the merger fraction, based on our measurements, declines rapidly at $z < 0.7$, although it appears roughly constant at $0.7 < z < 1.2$. This result is unlikely solely due to cosmic variance, as both fields show this behaviour, and this result is relatively insensitive to the exact corrections we apply for redshifts and k -corrections. This result is, within our errors, significant at $> 4-\sigma$, based on the combined EGS+COSMOS sample.

We also fit these two redshift ranges in the EGS+COSMOS merger fraction evolution separately, as shown in Figure 6 by the two dashed lines. Here we fit both the evolution at $z < 0.7$ and $0.7 < z < 1.2$ as power-laws, in which we find very different slopes. At $z < 0.7$ we find that the best fit power-law slope is $m = 5.2 \pm 1.0$ with $f_0 = 0.009 \pm 0.003$, going right through the de Propriis et al. (2007) $z = 0.05$ value. At $0.7 < z < 1.2$ the slope is $m = 0.07 \pm 0.55$, which indicates very little evolution, and therefore must be the result of significant merging activity within this epoch. We also see a turnover in the merger history at $z > 2$ (Conselice et al. 2008a), which has also been seen for galaxies in pairs at similar redshifts (Ryan et al. 2008).

Furthermore, Figure 7 compares our merger fractions with results from other merger fraction studies in Figure 7. Specifically, we compare our merger history with the results of both previous pair and structural studies. Points on Figure 7 include de Ravel et al. (2008) who use the VVDS to determine the pair fraction evolution for galaxies from $z = 0.5$ to $z = 1$. We plot on Figure 7 the results from this study for galaxies which have a pair separation of $< 20 h^{-1} \text{ kpc}$, and a velocity difference $\delta V < 500 \text{ km s}^{-1}$ within a magnitude range of $M_B < -18 - Q(z)$. The $Q(z)$ factor accounts for the evolution of stellar populations, and is an attempt to match the photometric evolution of galaxies so as to obtain the same galaxies at different redshifts. We also compare with recent DEEP2 results for the pair fraction evolution from Lin et al. (2008), who find similar pair fractions to de Ravel et al. (2008). The other pair fraction we compare with is Kartaltepe et al. (2007) who measure pair fractions within COSMOS within $< 20 h^{-1} \text{ kpc}$ separation using photometric redshifts. This paper finds 1749 galaxy pairs for systems brighter than $M_V = -19.8$, roughly equivalent to the stellar mass limit we have used. Finally, we compare our merger fractions to those published by Lotz et al. (2008a) using the Gini/ M_{20} method for 3009 galaxies within the EGS brighter than $0.4L_B^*$.

3.3.4 Extremely Massive Galaxies

In addition to systems selected by $M_* > 10^{10} M_\odot$, we also examine the evolution of the merger fraction for the extremely massive galaxies in our sample, those with $M_* > 10^{11} M_\odot$. There are several issues however when measur-

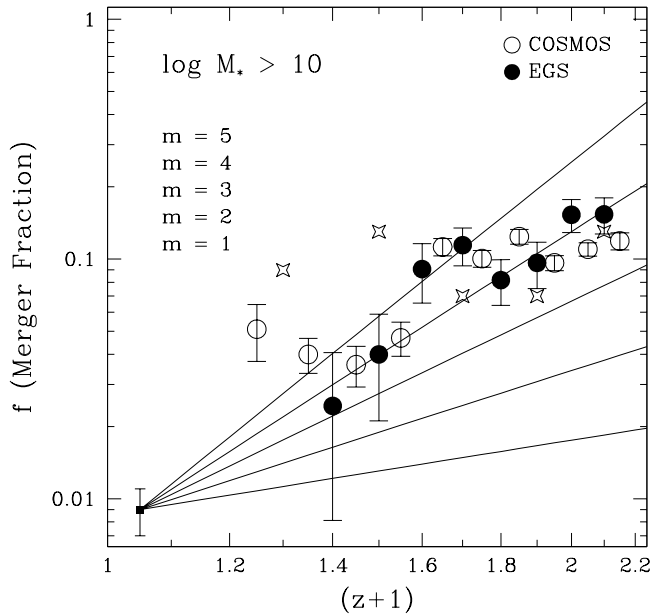


Figure 5. The evolution of the derived merger fraction up to $z = 1.2$ through the use of the CAS system for the EGS (solid circles) and COSMOS (open circles) fields. The open stars are the derived merger fractions from the EGS using the Gini/ M_{20} parameters from Lotz et al. (2008). The point at $z = 0.05$ originates from De Propriis et al. (2007). The five solid lines show the evolution from $z = 0.05$ as a power-law, with f_0 fixed to 0.009, and with various values of the power-law index shown; $m = 1, 2, 3, 4, 5$.

ing the merger fraction for these systems. The first is simply that there are not nearly as many galaxies with these masses as for systems selected by $M_* > 10^{10} M_\odot$. This can be seen in Figure 8, where at the lowest redshifts at $z \sim 0.3$ there are not enough systems to measure the merger fraction, and very few at $z \sim 0.4$, with resulting large error bars.

In any case, what we find is that the merger fractions for $M_* > 10^{11} M_\odot$ galaxies at $0.2 < z < 1.2$ overall are very similar to that for $M_* > 10^{10} M_\odot$ systems. It appears that at $z > 0.7$ the merger fraction for these extremely massive galaxies is slightly lower than for the $10^{10} M_\odot$ systems. This changes at lower redshifts where the $M_* > 10^{11} M_\odot$ galaxies appear to have slightly higher merger fractions, although we note that the error bars on these fractions do not rule out that these points are in fact as low, or even lower than, those for systems at $10^{10} M_\odot$.

3.3.5 Parameterisation of the Merger Fraction Evolution

There are a few popular ways to fit the merger fraction evolution. The first is the traditional power-law format (Patton et al. 2002; Conselice et al. 2003; Bridge et al. 2007) which dates back to early work by Zepf & Koo (1989) on the evolution of the merger fraction. This fitting format is given by,

$$f_m(z) = f_0 \times (1+z)^m \quad (10)$$

where $f_m(z)$ is the merger fraction at a given redshift, f_0 is the merger fraction at $z = 0$, and m is the power-law

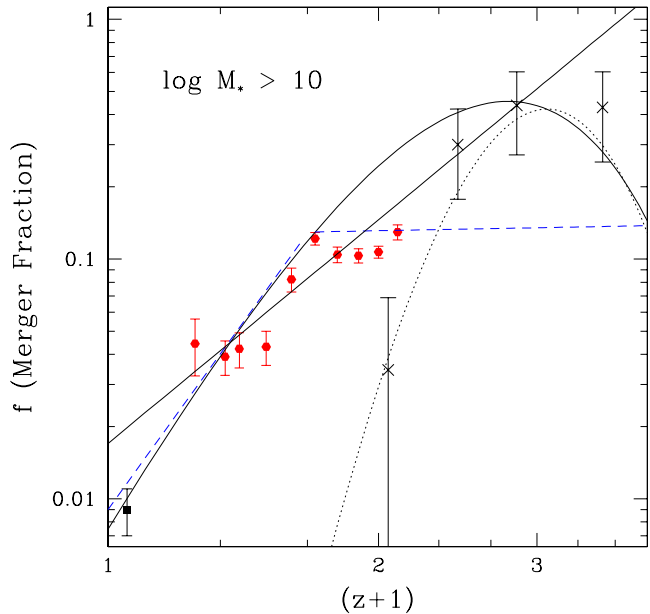


Figure 6. The evolution of the merger fraction from $z = 0$ to $z = 3$ using structural parameters from the CAS system. The point at $z = 0.05$ originates from the study of De Propriis et al. (2007). The points between $z = 0.4$ and $z = 1.2$ are from the combined EGS and COSMOS fields, which are plotted individually on Figure 5. The points from $z > 1$ (crosses) are taken from the CAS study of the Hubble Deep and Ultra Deep Fields (Conselice et al. 2008a). We show several fits as well, with the solid straight line the best fit power-law, while the curved solid line is the best fit for the combined exponential/power-law parameterisation (see text). Also shown as the two dashed blue lines are the best fit power-law parameterisation for the EGS+COSMOS points at $0.2 < z < 0.7$ and $0.7 < z < 1.2$, fit separately. This shows the rapid evolution in the merger fraction within $z < 1.2$. The dotted line shows the previous best fit exponential/power-law relation for galaxies with stellar masses $M_* > 10^{10} M_\odot$ described in Conselice et al. (2008a).

index for characterising the merger fraction evolution. Zepf & Koo (1989) calculated a merger fraction evolution which increased with redshift up to $z = 0.25$, and obtained a slope of $m = 4.0 \pm 2.5$. Nearly all further studies have found values within this range.

However there is currently a debate over the true nature of the increase, with some studies finding a fast evolution (Conselice et al. 2003; Kartaltepe et al. 2007), while others have found a more modest evolution (e.g., Lotz et al. 2008a; Lin et al. 2008). There are several reasons for this diversity in the parameterisation of the merger fraction evolution, which we discuss after demonstrating the various ways the merger fraction evolution can be fit within our own sample.

We explore below the power-law behaviour of the merger fraction evolution in a few ways. The first method is to investigate the power-law fit to the merger fractions solely within the COSMOS+EGS data set (Figure 5). When we fit a power-law to this evolution using just the points from COSMOS+EGS at $0.2 < z < 1.2$ we find a best fit given by $f_0 = 0.025 \pm 0.005$ and $m = 2.3 \pm 0.4$. That is, internal

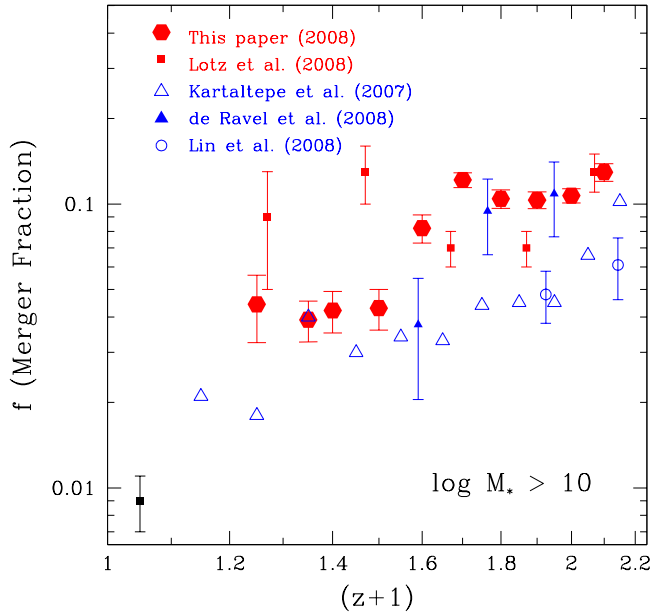


Figure 7. The evolution of the derived merger fraction through several previous studies compared to our results. Those systems which are coloured red are those derived through structural methods, either the CAS system (this paper) or the Gini/ M_{20} method (Lotz et al. 2008a). The blue symbols are the merger fractions derived from pair studies, either kinematic pairs as in Lin et al. (2008) and de Ravel et al. (2008) or photometric pairs from the COSMOS fields (Kartaltepe et al. 2007). In general the morphologically defined mergers give a higher merger fraction than those derived through pairs.

to itself, the CAS merger fraction from $z = 0.2$ to $z = 1.2$ increases modestly with time. Note that the derived merger fraction at $z = 0$ for this sample is 0.025 ± 0.005 which is about a factor of three larger than the $z = 0$ merger fraction derived from de Propriis et al. (2007). When we hold the $z \sim 0$ point at a constant value of $f_0 = 0.009$ we find that the best-fit slope for COSMOS+EGS data increases to $m = 3.8 \pm 0.2$.

Our derived evolution is similar to the results found by Lotz et al. (2008a), whose merger fractions are similar to ours (Figure 7). Our merger fraction evolution power-law slope, m , is however smaller than the index m measured by Kartaltepe et al. (2007) using pair counts. Even though Kartaltepe et al. (2007) find in general lower pair fractions compare to our merger fractions, the increase with time is more pronounced, and they derive an index of $m = 3.1 \pm 0.1$. This is more than $2\text{-}\sigma$ away from our result, and this difference deserves some explanation.

When we fit the Kartaltepe et al. (2007) points with the same $z = 0$ prior we use for the EGS+COSMOS data, we find that the best fit slope is $m = 2.9 \pm 0.1$. When we remove the $z \sim 0$ prior in this fit, we find that the slope changes to $m = 2.7 \pm 0.6$, although most of this is driven by the high redshift points from Kartaltepe et al. (2007). If we remove

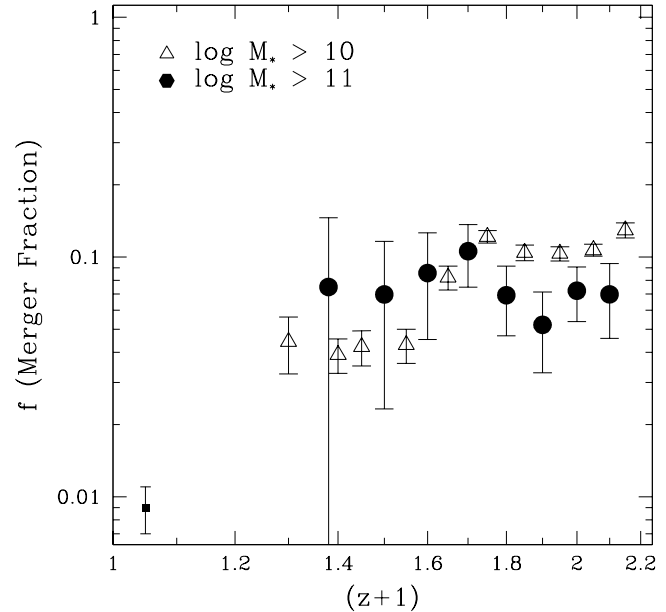


Figure 8. A comparison between the evolution of the merger fraction using the CAS method for galaxies with $M_* > 10^{10} M_\odot$ and $M_* > 10^{11} M_\odot$ from $z = 0.2 - 1.2$. In general we find that the evolution at higher masses is similar to those presented in the other plots in this paper, although the higher mass systems have a higher uncertainty associated with their measured merger fractions.

the highest redshift point (Figure 7), the measured value of $m = 1.8 \pm 0.3$, which is very similar to our own value at the same redshift range.

Overall, we find that the value of m can vary significantly depending on what value of f_0 is chosen. For example, if the $z = 0$ merger fraction for $\log M_* > 10$ galaxies is twice as high as the de Propriis et al. value (i.e., $f_0 = 0.018$) then the best fit value of the power-law slope changes from $m = 3.8 \pm 0.2$ to $m = 2.8 \pm 0.1$, thus raising the $z = 0$ merger fraction lowers the value of the power-law slope. If we hold the $z \sim 0$ merger fraction as 4%, then we find that the power-law slope falls to $m = 1.5 \pm 0.1$. Note that this does not appear to be the case for very massive galaxies with $M_* > 10^{11} M_\odot$ (Bluck et al. 2008).

Since the $z \sim 0$ merger fraction can be critically important for deriving the merger history if it is used as a prior, it is worth examining what the merger fraction at $z \sim 0$ is, and how certain we know this number. We also have some estimates of what the local merger fraction is from previous work such as Patton et al. (2000) and de Propriis et al. (2007). We use the Millennium Galaxy Catalog (MGC) selection for mergers, which is based on systems which are at $M_B < -18$, and thus a complete comparison is not possible without measuring the stellar masses for these galaxies.

De Propriis et al. (2007) find that the merger fraction at $z \sim 0.05$, is $f_0 = 0.009 \pm 0.02$, based on the CAS asymmetry. By holding the value of f_0 fixed to 0.009, we fit a power-law slope of $m = 3.8 \pm 0.2$. However, this is not a good fit to the data (Figure 6), and tends to under-predict the merger fraction at $z = 0.8$ and over-predict the fraction at $z > 0.8$.

One of the features of the derived merger fraction up to $z = 1.2$ is that between various neighboring redshifts there are significant differences in the derived merger fraction (Figures 5-7). This is true for the combined EGS+COSMOS sample, the EGS and COSMOS samples alone, and is also found for the Gini/ M_{20} approach in Lotz et al. (2008a), as well as the pair method derived in Kartaltepe et al. (2007). In fact, the slope of the power-law merger fraction evolution ranges from $m = 5$ to $m = -3$ between two neighboring individual merger fractions. It is not yet clear what the origin of these differences are, whether the result of cosmic variance, or systematics. However on average the merger fraction does increase slightly with time up to $z = 1.2$ (§3.3.3).

We do a similar examination of the best power-law fit to the merger fraction evolution by including higher redshift merger fractions taken from a combined UDF+HDF sample (Conselice et al. 2008a) selected with the same stellar mass cut of $M_* > 10^{10} M_\odot$. The resulting merger fraction evolution is shown in Figure 6, which is currently our best estimate of how the merger fraction varies with time for a mass selected sample. When we fit the merger fraction evolution for $M_* > 10^{10} M_\odot$ galaxies from $z = 0$ to $z = 3$ we find that the best fit using all points, and no priors, is: $f_0 = 0.015$ and $m \sim 3$, although this power-law fit is poor, and the χ^2 is large.

If we hold the value of $f_0 = 0.009$, we find that the best fit value of the power-law slope increases to $m = 3.7$, although this does not go through the highest redshift point, and results in a poor fit. However, the $z = 0$ extrapolation from the best fit to all the data predicts that the nearby merger fraction is roughly twice the best value we currently have. This again demonstrates the importance of the value of f_0 within the power-law fit. The value of f_0 determines to a large degree what the fitted slope of the power-law evolution will be, especially if the value is held constant during the fit.

Another way to characterise the merger fraction evolution, which dates back to theoretical arguments based on the Press-Schechter formalism for merging (Carlberg 1990), is a combined power-law exponential evolution. This form appears to be a better fit to all of the redshift data than a simple power-law (Conselice 2006b). This is however not the case for the merger fraction for $M_* > 10^{11} M_\odot$ galaxies at $z < 3$, which can be fit by a power-law (Bluck et al. 2009). The formula for the power-law/exponential evolution is given by:

$$f_m = \alpha(1+z)^m \times \exp(\beta(1+z)^2), \quad (11)$$

where the $z = 0$ merger fraction is given by $f_m(0) = \alpha \times \exp(\beta)$. We find in general that this combined exponential power-law fit is better than a simple power-law and is likely a better representation for how the merger fraction evolves with time. We also find this to be the case for a power-law/exponential form, without the square on the $(1+z)$ term in the exponential. However, none of these forms are

very satisfying, given the large errors on their fits, and the three free parameters needed to create the fit.

As discussed in Paper II (Conselice et al. 2009, submitted) there does not appear to be a simple way to parameterise the merger fraction. We explored several fitting routines, and found that the best-fit two parameter model is an exponential/power-law of the form:

$$f_m = \alpha(1+z)^3 \frac{1}{\exp(\beta \times z)}, \quad (12)$$

which is designed such that $f_0 = \alpha$, and is only a two parameter parameterisation, and fits the data as well as the three parameter model above. In any case, we have found that the fitting with the exponential/power-law and the Carlberg (1990) version of the exponential/power-law, gives an exponent on the power-law portion of $m \sim 3$. This is the index predicted for how the number densities of galaxies decline with redshift, and is therefore the natural exponent on the power-law for a passive merger evolution, which appears to occur at $z < 0.7$.

3.4 Comparison of Structural Mergers and Pair Fractions

One of the results we derive from our measured structural mergers is how the derived merger fractions, based on the CAS and other methods (such as Gini/ M_{20}), compare with derived pair fractions. Figure 7 shows this comparison, with the morphological methods (this work & Lotz et al. 2008a) shown in red, and the pair methods (Kartaltepe et al. 2007; Lin et al. 2008; de Ravel et al. 2008) shown in blue. What is immediately clear is that the structural methods, while agreeing quite well with each other, find a higher merger fraction than the pair methodology. There are several possible reasons for this.

While it is possible that one or both methods have systematics that result in inaccurately measured merger fractions, we first investigate what the time-scales for these methods are. This is an important question as these fractions differing can be partially, or entirely, explained if the time-scales for merging for the two methodologies are different. For example, if the time-scale for a 20 kpc pair to merge is half the time-scale sensitivity for an asymmetric galaxy, then we would expect the pair fraction to be half of the CAS merger fraction if both methods are tracing the same merger process. That is, the merger fraction for a given sample scales as the time-scale sensitivity of the method used to find mergers. Since the merger rates for the two methods should give the same result, then the ratio of the pair fraction to its merger timescale should be equal to the structural merger fraction divided by its time-scale, or:

$$\frac{f_{\text{pair}}}{\tau_{\text{pair}}} = \frac{f_{\text{CAS}}}{\tau_{\text{CAS}}}. \quad (13)$$

Time-scales (τ) within the merger process are notoriously difficult to measure, and have large uncertainties. Initially, measuring the merger rate from pairs involved dynamical friction calculations (e.g., Patton et al. 2002; Conselice 2006), and typical time-scales for a 20 kpc pair to merge are 0.5-1 Gyr with various assumptions. The time-scale calculation for dynamical friction used by Conselice (2006b), and in earlier studies are based on isothermal mass distributions

and the time-scale can depend highly on the mass of the galaxies, and the characteristic velocity of the system (e.g., Conselice 2006b, eq. 7).

Likewise, the time-scales for merging within the CAS system for dark matter dominated galaxies was found to be similar to the dynamical friction time-scales derived from an isothermal profile, and a galaxy with mass of $\sim 10^{10} M_{\odot}$. There are however problems with both of these calculations, which have already been alluded to above for the dynamical friction time-scale. The measured time-scales for the CAS method are found by Conselice (2006) to vary between $\sim 0.3 - 0.8$ Gyr, depending on viewing angle and the orbital parameters of the two galaxies in the pair. Also, the simulations used in Conselice (2006) are purely dark matter, and it is desirable to determine the CAS time-scale for systems with stars, star formation, and dust.

New simulations were recently analysed by Lotz et al. (2008b) in terms of CAS, Gini/ M_{20} , and pair selection for mergers. Lotz et al. (2008b) furthermore utilise simulations that include star formation and dust, and are currently by far the most thorough investigation into merger time-scales using both morphology and the time-scales for mergers to occur within a given pair separation from $20 h^{-1}$ kpc to $30 h^{-1}$ kpc, and $50 h^{-1}$ kpc.

Lotz et al. (2008b) find a variety of time-scales for their merger simulations depending on the type of merger and the type of galaxy. For their highest resolution simulation (SbcPPx10), they calculate a merger time-scale of $\tau_{\text{CAS}} = 0.94 \pm 0.13$ for the CAS methodology, and a time-scale of $\tau_{\text{pair}} = 0.15 \pm 0.18$ for galaxies to merge within a $20 h^{-1}$ kpc pair. This ratio of time scale, which we denote as $\kappa = \tau_{\text{CAS}}/\tau_{\text{pair}}$, is equal to $\kappa = 6.3$ for this model.

Figure 9 shows the histogram for the value of κ for all the models published in Lotz et al. (2008b). What we find is a general distribution, but with all the Sbc models having a ratio $\kappa > 1$. The models shown by the blue hatched histogram in Figure 8 are for the Lotz et al. ‘G’ models, which are less gas dominated, and have sub-parabolic orbits which lead to artificially shortened merger-times in pairs. As can be seen, while earlier analytical calculations showed that the time-scale for pair merging was similar to the morphological merger time-scale, the simulations by Lotz et al. demonstrate that the time-scales for pairs to merge are shorter than the analytical estimates.

This implies that if the pair method and the structural methods are measuring the same merger process, then the merger fractions derived from pairs should be lower than those derived from structure by an equivalent amount. We denote this ratio as $\kappa' = f_{\text{CAS}}/f_{\text{pair}}$. For the COSMOS field we find that the value of κ' using the data from Kartaltepe et al. (2007) and this paper, give κ' values from 1.5-3.5, yet the pairs from Kartaltepe et al. (2007) are not selected in the same way our CAS mergers are, i.e., with $M_{*} > 10^{10} M_{\odot}$.

A better test of the merger criteria time-scale is to determine how the ratio of the CAS merger fraction and the pair fraction change with redshift in the same sample and stellar mass selection. While it is likely that even within the same sample, the CAS and pair methods will find galaxies in different modes of evolution (De Propriis et al. 2007), it is still instructive to determine this ratio within a well defined

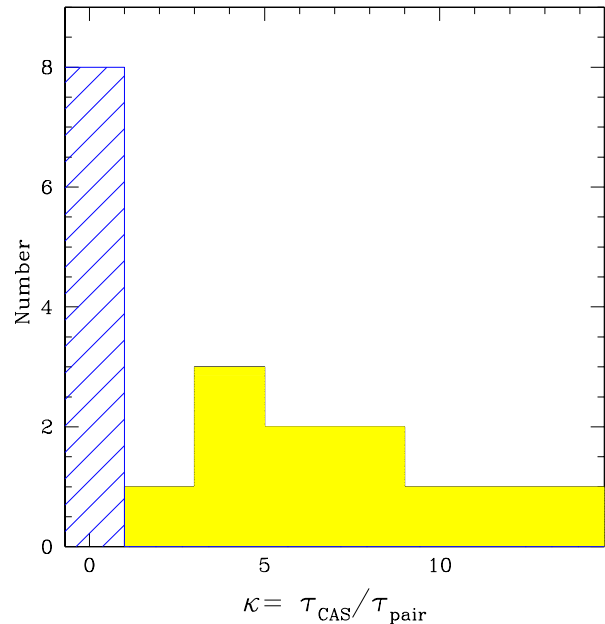


Figure 9. The ratio of the time-scale sensitivity for the CAS identified mergers and the time-scale for merging for galaxies in $20 h^{-1}$ kpc pairs (κ). The blue hatch histogram shows the results for galaxies in sub-parabolic orbits, while the solid yellow show the results for the more realistic Sbc orbital models from Lotz et al. (2008b).

sample. We utilize the POWIR database from the EGS to determine this ratio (e.g., Conselice et al. 2007b, 2008b).

Figure 10 shows this ratio for galaxies at separations of less than 20 kpc, 30 kpc, and 50 kpc. The values for $f_{\text{m}}(\text{CAS})/f_{\text{m}}(\text{Pair})$, with a pair defined as having a separation of < 20 kpc, range from 12.2 to 2.3, with a average value of 6.2, which perhaps coincidentally, is close to the value of κ for the highest resolution model from Lotz et al. (2008b). This implies that there is no inconsistency between the pair method and structural methods for measuring merger fractions and rates.

3.5 Merger Rates

We are now in a position to measure the galaxy merger rate for $M_{*} > 10^{10} M_{\odot}$ galaxies from $z = 0$ to $z = 3$. The merger rate is difficult to measure, however, and our attempt should be viewed as a preliminary full measure of this evolution up to $z = 3$. Measurements of the merger rate will improve as our understanding and knowledge of galaxy number densities, merger fractions, and merger times scales improve.

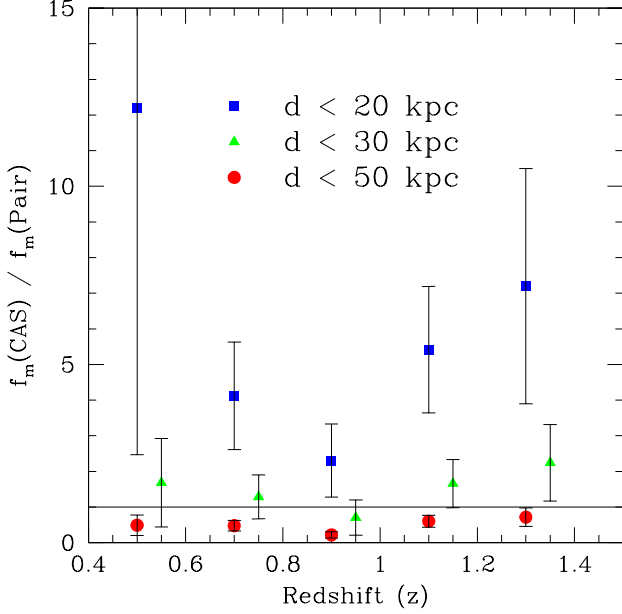


Figure 10. The ratio of the CAS merger fraction and the pair fraction, within the same sample of galaxies with $M_* > 10^{11} M_\odot$ within the EGS and the other POWIR fields (Conselice et al. 2007b, 2008b). The blue squares are for those systems with separations of < 20 kpc, the green triangles are for those with separations of < 30 kpc, and the red circles are for systems with separations of < 50 kpc.

3.5.1 Merger Rates per Galaxy

Since the merger rate has a relatively high error associated with it, we first investigate the merger rate per galaxy, which is simply just the number of mergers a galaxy of a given mass will undergo as a function of time. We, in fact, examine the inverse of this, which we call Γ , which is the average amount of time a galaxy exists before undergoing a merger as a function of redshift, or

$$\Gamma = \frac{\tau_m}{f_{gm}}, \quad (14)$$

where we have utilised the galaxy merger fraction, or rather the fraction of galaxies merging in a population, which is related to the merger fraction (f_m) by:

$$f_{gm} = \frac{2 \times f_m}{1 + f_m}. \quad (15)$$

In equation (14), we also use the time-scales for mergers (τ_m), which is potentially the largest uncertainty when trying to derive evolution from the merger fraction (§3.4). The value for τ_m is measured to range from $\tau = 0.4 - 1$ Gyr based on N-body models from Conselice (2006b) and from Lotz et al. (2008b). The nominal value we use, based on the average CAS time-scale using the Lotz et al. (2008b) SbcPP, SbcPR and SbcRR simulations is 1 Gyr, with an uncertainty in this

value of 0.3 Gyr. Note that this is more than a factor of two larger than the time-scale used in Conselice et al. (2008a), which utilised simulations from Conselice (2006) to derive a merger time-scale of 0.34 Gyr. The time-scale for a pair to merge, as found by Lotz et al. (2008b), is 0.2 ± 0.1 Gyr for a 20 kpc pair, and $\tau_m = 0.4 \pm 0.2$ Gyr for merging systems within the Gini- M_{20} system, which we also use to calculate the value of Γ , as plotted in Figure 11.

As can be seen in Figure 11, the typical value for Γ is around ~ 10 Gyr at $z < 1$, demonstrating that $z < 1$ galaxies with masses $M_* > 10^{10} M_\odot$ only undergo, on average, a single merger during this time. We can calculate the exact number of mergers that occur at $z < 3$ by integrating the inverse of Γ over redshift,

$$N_{\text{merg}} = \int_{t_1}^{t_2} \Gamma^{-1} dt = \int_{z_1}^{z_2} \Gamma^{-1} \frac{t_H}{(1+z)} \frac{dz}{E(z)}, \quad (16)$$

where t_H is the Hubble time, and $E(z) = [\Omega_M(1+z)^3 + \Omega_k(1+z)^2 + \Omega_\Lambda]^{-1/2} = H(z)^{-1}$. In this case, we parameterise Γ by:

$$\Gamma(z) = \Gamma_0(1+z)^m, \quad (17)$$

where we find a best fit of $\Gamma_0 = (13.8 \pm 3.1)$ Gyr, and $m = -1.6 \pm 0.6$. Using equation (16), and the parameterisation of Γ in equation (17) we calculate the number of mergers a galaxy with $M_* > 10^{10} M_\odot$ undergoes from $z = 3$ to $z = 0$. The total number of mergers depends strongly on the adopted value of the CAS merger time-scale (τ_m). The range in the total number of mergers a galaxy undergoes at $z < 3$ ranges from $N_{\text{merg}} = 2.3$ to 6.6, depending on the time-scale used. By integrating the individual merger fractions, we calculate that the total number of mergers a galaxy undergoes can be expressed as $N_{\text{merg}} = 2.3\tau_m^{-1}$ at $z < 3$. Most of the merging within these massive galaxies occurs at $z > 1$, independent of the value of the merger time-scale, as discussed in Conselice et al. (2008a).

The total number of cumulative mergers a galaxy undergoes from $z = 3$ to $z = 0$ is shown in Figure 12 for three different time-scales of CAS sensitivity to the merger process - $\tau_m = 0.35, 0.5, 1$ Gyr. Also shown in Figure 12, as the dashed line, is the evolution in the total cumulative number of mergers for a population with a constant $\Gamma = 1$ Gyr. Although the total number of mergers depends strongly on the still uncertain time-scale for the merger process, it is clear that most merging for massive galaxies must occur at $z > 3$. The horizontal line's intersection with the various models shows at which redshift a galaxy will on average have had a single major merger since $z = 3$. This varies between $z = 1.5$ to $z = 2.5$. Thus, independent of the time-scale used, on average, massive galaxies with $\log M_* > 10$ undergo a merger between $z = 2.5$ and $z = 1.5$. Likewise, at $z < 1$ (the vertical solid line), a typical massive galaxy will undergo between 0.5 to 2 major mergers, depending on the time-scale sensitivity. Our best estimate for the amount of stellar mass galaxies with $M_* > 10^{10} M_\odot$ grow by at $z = 1$ to $z = 0$, based on the evolution of the mass function, is a factor of ~ 2 increase (Conselice et al. 2007), demonstrating consistency between our findings and the actual evolution in stellar mass in galaxies.

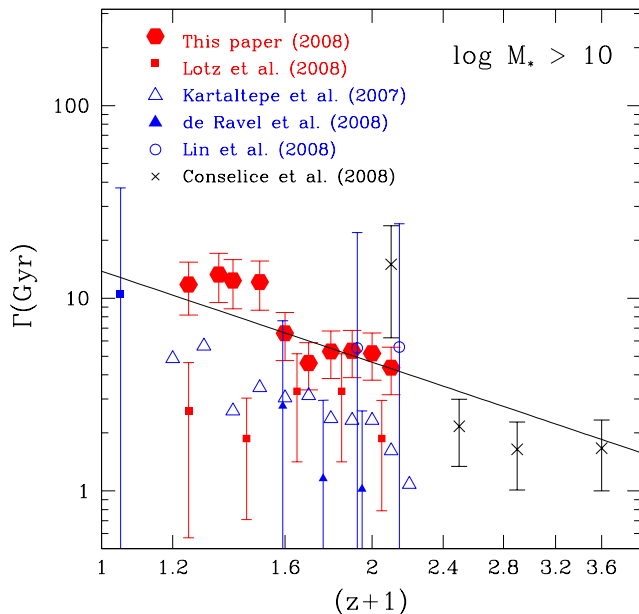


Figure 11. The evolution of the quantity Γ , which is the average time between a merger for galaxies with $M_* > 10^{10} M_\odot$ at $z < 3$. We include on this plot the measured pair fractions (e.g., Kartaltepe et al. 2007; de Ravel et al. 2008 and Lin et al. 2008). The merger fractions by which the value of Γ is calculated from galaxy structure, include those from this paper, and previous work by Lotz et al. (2008a) at $z < 1.2$, and Conselice et al. (2008a) for systems at $z > 1$. The solid line shows the best fit power-law evolution, which we use to parameterise Γ for measuring the cumulative merger history for $M_* > 10^{10} M_\odot$ galaxies.

3.5.2 The Galaxy Merger Rate

Another important physical quantity to obtain when studying galaxy mergers, is the galaxy merger rate ($\mathcal{R}_g(z)$), which is the number of galaxies merging, per unit time, per unit co-moving volume. The galaxy merger rates for our sample are calculated through the merger rate equation,

$$\mathcal{R}_g(z) = f_{gm}(z) \cdot \tau_m^{-1} n_{gm}(z) \quad (18)$$

where n_{gm} is the number density of galaxies within a given stellar mass range, and f_{gm} (eq. 15) is the galaxy merger fraction. Note that this is not the merger fraction, which is the number of mergers divided by the number of galaxies, which is roughly half the galaxy merger fraction (Conselice 2006). We obtain our galaxy number densities n_{gm} from Conselice et al. (2007b) for galaxies with stellar masses $M_* > 10^{10} M_\odot$ at $z > 0.2$, and from Cole et al. (2001) for galaxies at $z \sim 0$.

The resulting galaxy merging rate is shown in Figure 13. The galaxy merger rate increases with time for the $M_* > 10^{10} M_\odot$ galaxies, from $z = 0$ to $z = 3$. This slightly differs from the findings of Bluck et al. (2009) who find that the merger rate for $M_* > 10^{11} M_\odot$ galaxies is consistent with being constant from $z = 0$ to 3. We try to parameterise this evolution of the galaxy merger rate in various ways, and find

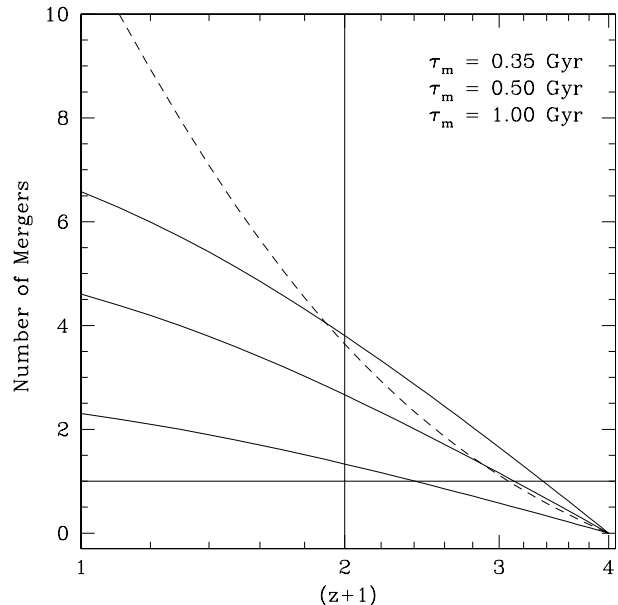


Figure 12. The integrated number of mergers since $z = 3$, as a function of the time-scale for CAS sensitivity to the merger process. The three solid lines show the evolution of how many mergers have occurred for galaxies with $M_* > 10^{10} M_\odot$ since $z = 3$ using different values for the time-scale in which the CAS system is sensitive to mergers (see text). The dashed line shows the evolution for mergers with a constant time-scale of $\Gamma = 1$ Gyr.

that a linear form of $R_g = C \times z + R_{g,0}$ gives the best fit (as shown by the solid line in Figure 13). However, as can be seen in Figure 13, this linear fit predicts that the merger rate should drop quicker at $z < 0.2$ than what is actually seen. This is potentially the result of either the merger rate dropping linearly from $z \sim 3$ until $z \sim 0.7$, and then dropping very quickly and remaining relatively constant at $z < 0.6$. It also could be the result of the time-scale for the pair measurements at $z \sim 0$ to be incorrect. If the time-scale were 0.4 Gyr, this would drop the merger rate by a factor of two for the $z \sim 0$ point, although this would still not alleviate the problem of matching with the rate of linear decrease seen at higher redshifts. The merger rates at $z < 0.5$ appear to be constant for $M_* > 10^{10} M_\odot$ galaxies.

The merger rate therefore decreases nearly linearly with redshift at $0.7 < z < 3$, whereas the merger fraction is relatively well fit as a power-law decrease over the same epoch. While the galaxy number densities for $M_* > 10^{10} M_\odot$ systems remains relatively constant at $z < 1$, they decline quickly at higher redshifts (e.g., Conselice 2007). This is matched, and then some, by the increased merger fraction, which produces a linear decline with decreasing redshift. It is possible, as for the case of very massive galaxies discussed in Bluck et al. (2009) for the number density de-

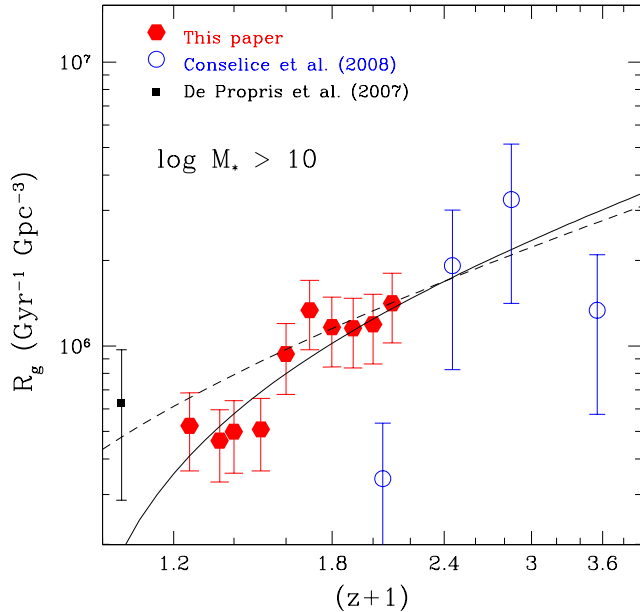


Figure 13. The galaxy merger rate (\mathcal{R}_g), defined as the number of galaxies undergoing a merger per unit time, per unit co-moving volume, as a function of redshift. Shown here are only systems with $M_* > 10^{10} M_\odot$, as measured by the CAS system from this paper at $0.2 < z < 1.2$; Conselice et al. (2008a) for $z > 0.6$ galaxies (blue circles), while the $z = 0.05$ is the rate derived from De Propriis et al. (2007).

cline to match the increased merger fraction, producing a relatively flat evolution of the merger rate.

The time integral of the merger rate gives us the number of mergers which have occurred per unit volume since $z = 3$. The result of this calculation for the number of mergers which have occurred in a 10 Mpc^3 co-moving cube is shown in Figure 14. The solid lines show the evolution for the same time-scales as in Figure 12. Clearly, the number of mergers in this volume, which contains roughly six galaxies today, increases rapidly at higher redshifts, but levels off at $z < 1$. Most of the merging in the universe, as found in previous work (e.g., Conselice et al. 2003; Lotz et al. 2008a), is at higher redshifts. As discussed in Bertone & Conselice (2009, submitted), this is in disagreement with Cold Dark Matter semi-analytical models, such that we are finding a higher merger rate at very high redshifts, compared with the simulations.

4 SUMMARY

We have carried out an analysis of the structural CAS parameters for a sample of $> 20,000$ galaxies with stellar masses $M_* > 10^{10} M_\odot$ within the EGS and COSMOS fields, between $z = 0.2$ and $z = 1.2$. We explore in this paper

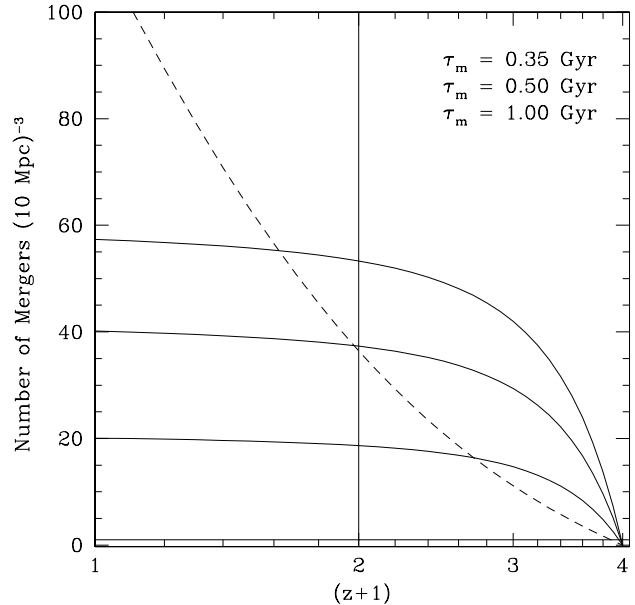


Figure 14. The integral of the galaxy merger rate (\mathcal{R}_g), from $z = 3$ to $z = 0$ over a volume of $(10 \text{ Mpc})^3$. This integral gives the total integrated number of mergers which have occurred within this volume since $z = 3$. As for the integral of Γ^{-1} (Figure 12), most of this merging occurs within a co-moving volume at higher redshifts, with roughly 20-60 mergers occurring at $z < 3$.

the merger fraction history, including various parameterisations, comparison of structural and pair merger fractions, the merger rate and role of mergers in galaxy formation, as well as systematics which are possibly playing a role in the derived merger fraction. The primary results from this paper are:

- I. We find through the CAS structural method that the merger fraction slightly increases from $z = 0.2$ to $z = 1.2$ with the merger fraction increasing from $f_m = 0.04 \pm 0.01$ to $f_m = 0.13 \pm 0.01$.
- II. We compare our derived merger fractions to previously published merger fractions from Lotz et al. (2008a) and pair studies from Kartaltepe et al. (2007), Lin et al. (2008) and de Ravel et al. (2008). Our results are comparable with the Gini/ M_{20} derived merger fractions from Lotz et al. (2008a), but we find our merger fractions are between 3-6 times higher than those derived from pairs, even within the same stellar mass selection. We argue this in some detail through the use of a $M_* > 10^{11} M_\odot$ sample of galaxies in the EGS. We also show that this ratio of structural mergers and pair fractions is however predicted in the latest N-body models of galaxy mergers from Lotz et al. (2008b) and is due to differing merger time-scales.
- III. We investigate various methods, including the use of pri-

ors, for parameterising the merger history through the CAS method. We show that the power-law formalism, whereby the merger fraction is parameterised by $f(z) = f_0 \times (1+z)^m$, is a poor fit to the merger fractions at $z < 1$. We further show that the value of the power-law slope, m , can vary depending on whether a prior is used to set the local $z = 0$ merger fraction. If we fit only our $z = 0.2 - 1.2$ merger fractions from COSMOS+EGS we fit a merger fraction evolution of $f(z) = 0.025 \pm 0.005(1+z)^{2.3 \pm 0.4}$. However, by using a prior of $f_0 = 0.009$ from de Propriis et al. (2007), the slope of the power-law fit is $m = 3.8 \pm 0.2$

IV. We find that a combined power-law exponential is a better fit to the merger fraction at $z < 3$ than just a simple power-law. We fit this form to the merger fraction using a $z = 0$ prior, and without, finding a similar form that predicts a turnover in the merger fraction for $M_* > 10^{10} M_\odot$ galaxies at $z = 2$.

V. We calculate the merger rate by using the latest measures of merger time-scales from merger simulations, and number densities for galaxies with $M_* > 10^{10} M_\odot$ from Conselice et al. (2007b). Although the errors on measuring the merger rate are large, resulting from uncertainties in the merger fraction, the merger time-scale, and the galaxy density, it is the ultimate quantity, and can reveal the role of mergers in forming galaxies. We find that the merger rate is roughly constant up to $z = 0.7$, and increases at $z > 1$ by a factor of 10. We also show that the merger rate for $M_* > 10^{10} M_\odot$ galaxies can be parameterised up to $z \sim 2$ as a linear increasing function.

We thank the staff at the Palomar and Keck observatories for invaluable assistance in collecting the data used for the Extended Groth Strip survey. Funding to support this effort came from a National Science Foundation Astronomy & Astrophysics Fellowship, and grants from the Science Technology Facilities Council (STFC). Support for the ACS imaging of the EGS in GO program 10134 was provided by NASA through NASA grant HST-G0-10134.13-A from the Space Telescope Science Institute, which is operated by the Association of Universities for Research in Astronomy, Inc., under NASA contract NAS 5-26555.

REFERENCES

- Arp, H. 1966, *ApJS*, 14, 1
- Barton, E.J., Geller, M.J., Kenyon, S.J. 2000, *ApJ*, 530, 660
- Benitez, N. 2000, *ApJ*, 536, 571
- Bershady, M.A., Jangren, J.A., Conselice, C.J. 2000, *AJ*, 119, 2645
- Bridge, C., et al. 2007, *ApJ*, 659, 931
- Bruzual, G., Charlot, S. 2003, *MNRAS*, 344, 1000
- Bluck, A., Conselice, C.J., Bouwens, R.J., Daddi, E., Dickinson, M., Papovich, C., Yan, H. 2008, *arXiv:0812.0926*
- Bundy, K., Fukugita, M., Ellis, R., Kodama, T., Conselice, C.J. 2004, *ApJ*, 601, 123L
- Bundy, K., et al. 2006, *ApJ*, 651, 120
- Bundy, K., Ellis, R.S., Conselice, C.J. 2005, *ApJ*, 625, 621
- Carlberg, R. 1990, *ApJ*, 359, 1L
- Cassata, P., et al. 2005, *MNRAS*, 357, 903
- Cole, S., et al. 2001, *MNRAS*, 326, 255
- Conselice, C.J., Bershady, M.A., Jangren, A. 2000a, *ApJ*, 529, 886
- Conselice, C.J., Bershady, M.A., Gallagher, J.S. 2000b, *A&A*, 354, 21L
- Conselice, C.J., Gallagher, J.S., Calzetti, D., Homeier, N., Kinney, A. 2000c, *AJ*, 119, 79
- Conselice, C.J. 2003, *ApJS*, 147, 1
- Conselice, C.J., Bershady, M.A., Dickinson, M., Papovich, C. 2003a, *AJ*, 126, 1183
- Conselice, C.J., Chapman, S.C., Windhorst, R.A. 2003b, *ApJ*, 596, 5L
- Conselice, C.J., Gallagher, J.S., Wyse, R.F.G. 2002, *AJ*, 123, 2246
- Conselice, C.J., et al. 2004, *ApJ*, 600, 139L
- Conselice, C.J., Blackburne, J., Papovich, C. 2005a, *ApJ*, 620, 564
- Conselice, C.J., Bundy, K., Ellis, R., Brichmann, J., Vogt, N., Phillips, A. 2005b, *ApJ*, 628, 160
- Conselice, C.J. 2006a, *MNRAS*, 373, 1389
- Conselice, C.J. 2006b, *ApJ*, 638, 686
- Conselice, C.J., et al. 2007a, *ApJ*, 660, 55L
- Conselice, C.J., et al. 2007b, *MNRAS*, 381, 962
- Conselice, C.J., Rajgor, S., Myers, R. 2008a, *MNRAS*, 386, 909 (paper I)
- Conselice, C.J., Bundy, K., U., V., Eisenhardt, P., Lotz, J., Newman, J. 2008b, *MNRAS*, 383, 1366
- Davis, M., et al. 2003, *SPIE*, 4834, 161
- Davis, M., et al. 2007, *ApJ*, 660, 1L
- De Propriis, R., Conselice, C.J., Driver, S.P., Liske, J., Patton, D., Graham, A., Allen, P. 2007, *ApJ*, 666, 212
- de Ravel, L., et al. 2008, *arXiv:0807.2578*
- Ellison, S.L., Patton, D.R., Simard, L., McConnachie, A.W. 2008, *AJ*, 135, 1877
- Giallisco, M., et al. 2004, *ApJ*, 600, 93L
- Hernandez-Toledo, H.M., Avila-Reese, V., Conselice, C.J., Puerari, I. 2005, *AJ*, 129, 682
- Holmberg, E. 1941, *ApJ*, 94, 385
- Kampanyik, P., et al. 2007, 172, 329
- Kassin, S., et al. 2007, *ApJ*, 660, 35L
- Kawata, D., Mulchaey, J.S., Gibson, B.K., Sanchez-Blazquez, P. 2006, *ApJ*, 648, 969
- Kartaltepe, J.S., et al. 2007, *ApJS*, 172, 320
- Lanyon-Foster, M.M., Conselice, C.J., Merrifield, M.R. 2007, 380, 571
- Le Fevre, O., et al. 2000, *MNRAS*, 3111, 565
- Lin, L., et al. 2004, *ApJ*, 617, 9L
- Lin, L., et al. 2008, *ApJ*, 681, 232
- Lotz, J.M., et al. 2008a, *ApJ*, 672, 177L
- Lotz, J.M., et al. 2008b, *arXiv:0805.1246*
- Maraston, C. 2005, *MNRAS*, 362, 799
- Mobasher, B., et al. 2007, *ApJS*, 172, 117
- Papovich, C., Dickinson, M., Giallisco, M., Conselice, C.J., Ferguson, H.C. 2005, *ApJ*, 631, 101
- Patton D.R., Carlberg, R.G., Marzke, R.O., Pritchet, C.J., da Costa, L.N., Pellegrini, P.S. 2000, *ApJ*, 536, 153
- Patton D.R., et al. 2002, *ApJ*, 565, 208
- Ravindranath, S., et al. 2004, *ApJ*, 604, 9L
- Ravindranath, S., et al. 2006, *ApJ*, 652, 963
- Ryan, R.E., Jr., Cohen, S.H., Windhorst, R.A., Silk, J. 2008, *ApJ*, 678, 751
- Stanford, S.A., Dickinson, M.E., Postman, M., Fergu-

- son, H.C., Lucas, R.A., Conselice, C.J., Budavari, T., Somerville, R. 2004, AJ, 127, 131
- Taylor-Mager, V., Conselice, C., Windhorst, R., Jansen, R. 2007, ApJ, 659, 162
- Vorontsov-Velyaminov, B.A. 1959, "Atlas and Catalog of Interacting Galaxies", 1959, Sternberg Institute, Moscow: Moscow State University
- Windhorst, R., et al. 2002, ApJS, 143, 113
- Zamojski, M.A., et al. 2007, ApJS, 172, 468
- Zepf, S.E., Koo, D.C. 1989, ApJ, 337, 34